Second Order Photon Emission in Nuclei - Case of ^{137}Ba

A Thesis Submitted to the

College of Graduate Studies and Research

in Partial Fulfillment of the Requirements

for the degree of Master of Science

in the Department of Physics and Engineering Physics

University of Saskatchewan

Saskatoon

By

Ronan O. Lefol

©Ronan O. Lefol, October 2014. All rights reserved.

Permission to Use

In presenting this thesis in partial fulfillment of the requirements for a Postgraduate degree from the University of Saskatchewan, I agree that the Libraries of this University may make it freely available for inspection. I further agree that permission for copying of this thesis in any manner, in whole or in part, for scholarly purposes may be granted by the professor or professors who supervised my thesis work or, in their absence, by the Head of the Department or the Dean of the College in which my thesis work was done. It is understood that any copying or publication or use of this thesis or parts thereof for financial gain shall not be allowed without my written permission. It is also understood that due recognition shall be given to me and to the University of Saskatchewan in any scholarly use which may be made of any material in my thesis.

Requests for permission to copy or to make other use of material in this thesis in whole or part should be addressed to:

Head of the Department of Physics & Engineering Physics
116 Science Place, Rm 163
University of Saskatchewan
Saskatoon, Saskatchewan
Canada
S7N 5E2

Abstract

The two-photon decay in nuclei has been formally theorized for many years and attempted to be measured on numerous occasions. The special case of a $0^+ \rightarrow 0^+$ transition in nuclei was examined for certain isotopes, and a branching ratio for the two-photon decay determined for each isotopes. Measurements of the branching ratio in nuclei other than this special case had so far proven unsuccessful. Motivated to find the two-photon branching ratio in a case where the transition competes with the single photon transition, we study the $11/2^-$ ^{137}Ba isomer. The experiment was performed at the Technische Universität Darmstadt using the available $LaBr_3$ scintillation detectors.

We first study the absorption of various gamma energies by lead and compare the resulting values to a GEANT4 simulation. With an ideal value for lead shield thickness, the experimental setup is built in order to obtain a high two-photon count rate, while suppressing direct Compton scattering between detector pairs and suppressing other background interference. In order to suppress the background, plastic scintillators were placed atop the experimental setup. To treat the daunting level of random coincidences measured with this setup, fine energy and time gates were placed on the processed events in order to limit observation to the region of interest.

Throughout the experiment, three different detector pair angles were successfully examined: 72°, 120°, and 144°. With these three angles a partial representation of the angular distribution of the two-photon decay is observed. The branching ratios were measured to be $1.56(23) \cdot 10^{-6}$, $0.55(22) \cdot 10^{-6}$, and $0.70(18) \cdot 10^{-6}$ for the angles of 72°, 120°, and 144° respectively, with the values of 72° and 144° recorded in Ref.[1]. This experiment therefore shows it is possible to obtain a value for the two-photon branching ratio in the $11/2^-$ excited state of ^{137}Ba . A precise determination of this value, and for that of other nuclei, might contribute to solve current fundamental open problems such as restricting the parameters of the equation of state, or accurately determining neutron skin thickness.

Acknowledgements

At this point, I would like to offer thanks to those who have aided me in making this project possible.

I would first like to acknowledge my supervisor, **Professor Chary Rangacharyulu**. Throughout the entire process, Chary has kept pushing me further and further into the understanding of each and every concept. Not allowing for any shortcuts or unfounded answers, he has continuously pushed me to a greater understanding of the project and of the thought process one should take for a task such as this thesis.

I wish to offer my sincere thanks to **Prof. Dr. Peter von Neumann-Cosel** and **Prof. Dr. Norbert Pietralla** for making the process of me working at the Technische Universität Darmstadt a painless effort and their continued interest in the project. As well, a special thanks to Prof. Dr. Norbert Pietralla for allowing me to work within his work group to complete this project.

I also wish to thank **Dr. Heiko Scheit** for his technical expertise and support throughout the project.

I am as well indebted to **Dr. Christopher Walz** for his continuous help and assistance in the project. His aid and previous work on the DAQ and ADC construct architecture were invaluable for the completion of this project.

I wish to thank **Dr. John Millener** for his generous sharing of experimental and theoretical results concerning the two-photon decay in ^{137}Ba .

I finally wish to thank my friends in the Department of Physics and Engineering Physics, ever present, and always willing to lend a hand. You are all without a doubt the key factor in making my work environment a truly fun and amusing place to be.

The present work was supported by funds from the German Research foundation through SFB634. As well funding from the International Research Exchange Program (IREP) allowed for easier travels between the University of Saskatchewan and the Technische Universität Darmstadt.

Contents

List of Tables

List of Figures

List of Abbreviations

$LaBr_3$	Lanthanum(III) bromide
NaI	Sodium iodide
QED	Quantum Electrodynamics
IC	Internal Conversion
IPC	Internal Pair Conversion
IBM	Interacting Boson Model
IPM	Independent-Particle Model
qq	Quadrupole-Quadrupole
do	Dipole-Octupole
CFD	Constant Fraction Discriminator
ADC	Analog to Digital Converter
FPGA	Field Programmable Gate Array
VME	Versa Module Europa
NIM	Nuclear Instrumentation Module
DAQ	Digital Acquisition System
DDR	Double Data Rate
NIST	National Institute of Standards and Technology
LOF	List of Figures
LOT	List of Tables

Chapter 1

Introduction

In the domain of nuclear structure, electromagnetic transitions play a very important role. These transitions are often represented as real or virtual photons emitted from excited states in nuclei, or absorbed photons. These emitted photons carry with them crucial information about the transition occurring between the initial excited and final states such as energy, spin, and parity. Through the study of these emitted photons, it is possible to determine the energy levels and spin values for the states resulting from an isotope decay. The single real photon emission is the most commonly discussed electromagnetic transitions, however it has long since been known that the single photon emission is only a first order approximation of an electromagnetic de-excitation represented in QED. For many cases, the single photon has sufficed to describe physical concepts, however it is important to remember it does not comprise the entirety of the photon decay theory.

Obtaining a precise value for these higher order processes, such as the two photon emission, would allow for a better understanding of the nuclear structure and nuclear interactions. It would then necessary to measure the effect of such a contribution on the current electromagnetic processes. At present, values such as the decay rate of an excited state take only first order effects in consideration. The measured decay rate through two-photon emission would need to be taken into account for higher precision calculations. An estimation of a physical concept on the same order, or smaller, than that of the two-photon branching ratio would need to take such an effect in consideration. Failure to due as such would create an incomplete model of the estimated process.

As the single photon decay stems from the first order approximation, it is natural to expect a two-photon emission representing the second order approximation. Along these lines, studies have been performed by examining the two-photon decay in a $0^+ \rightarrow 0^+$

transition, and have successfully determined values for the two-photon branching ratio in certain isotopes [6]. In such a state, the single photon emission is forbidden by angular momentum conservation. This particular transition requires there to be a total angular momentum change of zero, however the photon is defined as having a unity spin. It is therefore impossible for a single photon to 'carry away' a spin change of zero due to angular momentum conservation. Considering only photon decays, the most likely candidate is then the two-photon decay, where it is possible for both photons to carry away opposing angular momentum, creating an effective zero change in momentum. Isotopes such as ^{16}O, ^{90}Zr, and ^{40}Ca satisfy this particular $0^+ \rightarrow 0^+$ transition.

The next step in the examination of the two-photon decay is evidently to study the decay in a situation where the single photon decay is not forbidden. Measuring the branching ratio for the two-photon decay in such a case would provide a new observable unique to each nucleus. It is suggested that the situation where the single photon decay is hindered, not forbidden, would present a good starting point. A prime example of isotopes with a hindered single photon decay are called isomers. These particular nuclei possess a much larger spin difference between both the initial and final states of the de-excitation than other nuclei. Due to this large spin difference, the single photon decay occurs less often, effectively hindering the process. Amongst such isomers, is the excited state of ^{137}Ba which is populated from ^{137}Cs, a very commonly utilized and easy to access radioactive source.

Previous experiments in this matter have proven unsuccessful due to the limited capability of filtering out the necessary background and random coincidences occurring from the environment, as well as from the single photon emission of the studied radioactive source. The key limiting experimental factors have been set by detector dead time, time resolution, and energy resolution.

With new advances in scintillation detectors and digital signal processing, the experiment now becomes more feasible. Utilizing the tools available at the Technische Universität Darmstadt, including multiple recently available $LaBr_3$ scintillation detectors, and a 250 MHz digitizer, it is deemed possible to overcome the previous experimental limitations. Amongst these limitations is the daunting background events created by Compton

scattering. These tools allow for a much more precise time and energy resolution, as such it is believed that it will be possible to overcome the experimental hurdle which has so far prevented the investigation of a possible two-photon decay branching ratio in ^{137}Ba .

1.1 Layout of Thesis

The remainder of this thesis is organized as follows. In Chapter 2 the theoretical background for the two-photon and relevant concepts are discussed. The theory begins by discussing the single photon decay, and continuing into the subject of interest, the two-photon decay. Previous studies, and the history of this decay, are presented within this chapter in order to present a complete background on the matter. The theoretical reasoning for choosing the ^{137}Ba isomer to perform the experiment is also described.

The experimental considerations in order to properly perform the experiment are described in Chapter 3. The physical constraints presented by this experiment are detailed in this chapter, as well as the methods utilized to overcome them. The experimental benefits of utilizing a radioactive ^{137}Cs source is also explained. Amongst these constraints is the discussion of the minimum lead shield thickness required for this experiment to attenuate Compton scattered photons which would cause 'fake' events. The experimental benefits of selecting the ^{137}Ba isomer, as well as a description of the setup are developed within this chapter.

Chapter 4 begins by explaining the In Situ energy calibration and efficiency determination performed during the experiment and their subsequent effects. The method by which time random coincidences and background counts are treated is developed afterward. The timing analysis performed is set to demonstrate that the observed peak at 661.7 keV is indeed due to the two-photon decay as opposed to Compton scattering. Finally the determination of the branching ratio is demonstrated.

A summary of the project as well as recommendations for further studies in this project are given at the end of this thesis.

Chapter 2

Theoretical Background

Radioactive decays through single photon emission is a common, and well understood electromagnetic decay process. Gamma decay from radioactive sources often occurs after a radioactive nucleus emits an α (two protons and two neutrons bound together) or β (electron or positron) particle and decays into a daughter isotope. This daughter isotope is often left in an excited state, that is the isotope is prone to emit a gamma-ray in order to lower its energy level. As a general rule, the nuclei de-excitation requires 10^{-12} seconds, making the gamma decay effectively instantaneous. Other means of de-excitation for the nuclei are possible, amongst which are internal conversion and internal pair production.

The single photon decay represents a first order process in Quantum Electrodynamic. The first order photon decay is demonstrated in Figure 2.1 (diagram a) as a feynman diagram. This diagram demonstrates an initial excited state ($|i\rangle$) moving forward in time, at a given point a single photon is emitted $|k\rangle$, leaving the nucleus in a lower energy, final state ($|f\rangle$). Although these states are labeled 'initial' and 'final' state it is important to understand that these labels are with respect only to the photon emission $|k\rangle$. It is common for certain isotopes to decay via multiple states, leading to a possible confusion with the labels 'initial' and 'final' states.

At the present moment, only the case of single photon emission is of interest. The cases demonstrated in diagrams b-d of Figure 2.1 representing the two-photon decay, will be discussed at a later time. It is primarily important to understand the first order single photon emission before studying the second order process. It is important to understand the characteristics of a given photon imposed by the structural details of the system. The system itself, in this case the isotope's initial excited and final states, is the governing factor in the emitted photon characteristics. This is due to the unique angular quantum

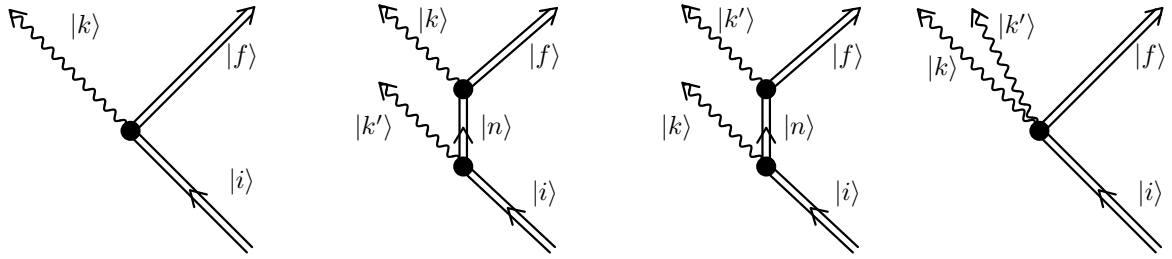

Figure 2.1: Feynman diagrams for the one photon decay(a) and the two-photon decay (b-d). (b-c) represent the second order resonance amplitudes, while (d) is the first order 'seagull' amplitude. (Taken from [1]

number change, type of transition, multipolarity of the transition, and energy level of the initial and final states.

2.1 Multipole Radiation

For any given nucleus, there are three types of electromagnetic decays, γ-ray emission, internal conversion , and internal pair conversion. In each of these cases the neutron and proton number within the isotope will remain the same. The de-excitation proceeds through emission of energy, thus lowering the excitation energy of the nucleus while leaving it physically constant. The majority of the γ-ray transition energy will be transmitted through an emitted photon while a small fraction of the energy will be lost in the nucleus recoil. In the case of γ-ray transitions, the energy lost through nucleus recoil is often considered insignificant with respect to the sum energy of the transition. The full transition energy, in this case the energy of the emitted photon, will total the energy difference between the initial excited state and the final state.

For any γ-ray emission occurring from a nuclei, the transition rate (λ) of that reaction depends on two factors: The type of radiation mechanism and the angular momentum carried by the photon [2]. It is important to note that photons are particles with zero mass and unit spin, with spin orientation either parallel or antiparallel to its momentum (helicity h=$\pm$1). Thus there can only be two photon states of a given momentum, $\hbar\mathbf{q}$. As such there are no single photon states with angular momentum number equal zero

($\ell = 0$), since this would imply a photon with helicity h=0.

For an electromagnetic transition originating from an initial state with angular momentum quantum number j_i, to a state with angular momentum quantum number j_f, the photon angular momentum quantum number (ℓ) is constrained by

$$|j_i - j_f| \leq \ell \leq j_i + j_f \tag{2.1}$$

The radiation occurring from this transition can be either due to an oscillation in charge distribution (Electric radiation), or an oscillation in current distribution (Magnetic transition). The transition rate for Electric radiation is represented as [2]

$$\lambda_E(\ell m) = \frac{2(\ell+1)}{\hbar\epsilon_0 \ell \left[(2\ell+1)!!\right]^2} \left(\frac{\omega}{c}\right)^{2\ell+1} |Q_{lm}|^2 \tag{2.2}$$

where Q_{lm} is a multipole matrix element between the initial (ψ_i) and final states (ψ_f). $\hbar$ represent the reduced plank's constant, ϵ_0 represents the permittivity of free space, and ω represents the energy of the emitted photon. Q_{lm} is defined as

$$Q_{lm} = e \sum_{k=1}^{Z} \int r_k^\ell Y_{\ell m}^*(\theta_k, \phi_k) \psi_i^* \psi_f dV \tag{2.3}$$

with $Y_{\ell m}^*(\theta_k, \phi_k)$ being the spherical harmonic function, and r_k^ℓ representing the radial wavefunction. Similarly, for the magnetic transition the transition rate is found as [2]

$$\lambda_M(\ell m) = \frac{2(\ell+1)\mu_0}{\hbar\ell \left[(2\ell+1)!!\right]^2} \left(\frac{\omega}{c}\right)^{2\ell+1} |M_{lm}|^2 \tag{2.4}$$

Regardless of the transition type, magnetic or electric, the photon angular quantum number describes another important characteristic of the transition. By understanding the possible values of ℓ determined via Equation 2.1, it is possible to determine the possible multipolarity values through which the transition will proceed.

$\ell = 1$ Dipole radiation

$\ell = 2$ Quadrupole radiation

$\ell = 3$ Octupole radiation

ℓ 2^{ℓ}-pole radiation

In addition to an angular momentum change, a change in energy state is often accompanied by a change in parity (from π_i to π_f). For these types of transitions, parity is always conserved. As there is a parity difference between the initial and final state, it is evident that the change in parity 'information' must be carried away by the emitted photon. Knowing both the parity and angular momentum quantum number for the photon, one may then determine the type of transmission through which the decay proceeds, as seen from [7]

$$\pi_\gamma = \begin{cases} (-1)^{\ell} & E\ell \\ (-1)^{\ell+1} & M\ell \ . \end{cases} \tag{2.5}$$

For example, the case where $\ell = 1$, i.e the dipole radiation, the parity of the photon for a magnetic dipole transition, would be $\pi_\gamma = +1$. In the case of an electric dipole transition, the photon parity would then be $\pi_\gamma = -1$.

As a general rule, lowest multipole order transitions are the most probable to occur. That is, low order multipole transitions have a higher transition rate (λ) compared to higher multipole transitions. In addition, Electric transitions have a faster transition rate than their Magnetic counterparts of the same angular momentum quantum number. These characteristics can be observed from Equation 2.2 and Equation 2.3. Although these general rules are useful to determine the likelihood of a particular transition happening prior to another, a specific value for the states transition rates is required in order to obtain precise results.

In order to obtain a correct estimation of these transition rates, three base assumptions must first be made. It is first assumed that the initial and final states are single particle wave functions derived from a spherical potential. Secondly, that the final energy state is an S-state, and finally that the radial wave functions are constants equal to $\sqrt{3}R_0^{-3/2}$ over the nuclear volume and zero outside the nucleus. By satisfying these three assumptions,

one may obtain the Weisskopf estimates for the gamma-ray transition rates [2].

ℓ	λ(E-ℓ)(s^{-1})	λ(M-ℓ)(s^{-1})
1	$1.02 \times 10^{14} A^{2/3} E_\gamma^3$	$3.15 \times 10^{13} E_\gamma^3$
2	$7.28 \times 10^{7} A^{4/3} E_\gamma^5$	$2.24 \times 10^{7} A^{2/3} E_\gamma^5$
3	$3.39 \times 10^{1} A^{2} E_\gamma^7$	$1.04 \times 10^{1} A^{4/3} E_\gamma^7$
4	$1.07 \times 10^{-5} A^{8/3} E_\gamma^9$	$3.27 \times 10^{-5} A^{2} E_\gamma^9$

Table 2.1: Weisskopf estimates, (E_γ is in units of MeV) [2]

It is important to note that the Weisskopf estimates are only a rough estimate, none the less they provide useful information on the transition probabilities. For these estimates, only the nuclear charge, mass number, and gamma energy are used in the determination of the estimates. By observing the variations between measured decay rates and the Weisskopf estimates, one can develop insight into which characteristics of the nuclei affect the decay.

An important characteristic these estimates demonstrate is the reduced decay-rate for higher values of angular momentum quantum number (ℓ). That is, a state decaying via a M4 transition will have a longer life time than a state decaying via an M1 transition. In addition, the estimates demonstrate the same behavior for the transition rates of electric versus magnetic transition as previously described. Limiting ourselves to the values shown in Table 2.1, it is clear that the E1 transition will be the most frequent, while the M4 transition will be the least likely.

Due to this observed variation in state half-life, it is 'easier' for low multipole transitions to occur than higher multipole transitions. In other words, low multipole transitions act as dominant transitions versus higher multipole transitions. There is of course still a probability for any transition to occur through a higher multipole transition, however this transition probability will be suppressed to favor the lowest multipole transition possible by the system.

The case of electric monopole transitions (E0) is worth noting in particular. A transition of type E0 may occur when both the excited and de-excited states of a nuclei are the same, such as 0^+, 1^+, etc... The first consequence of having a $0^+ \rightarrow 0^+$ transition is that the single photon decay is prohibited by angular momentum conservation as this would

require a $\Delta\ell = 0$, which as stated previously is not possible for a single photon. One may then imagine it is possible for the nucleus to decay via particle emission, however in many cases this is not energetically possible. In such a scenario, the decay will proceed through one of three methods. The first decay method is Internal Conversion, where one of the electrons, typically in the S-orbital state, interacts with the excited nucleus and is ejected from the atom. The emitted electron will carry away the total energy of the transition minus the energy required for the electron to escape the atom. Internal Pair Production is the second possible decay method where the transition energy is converted directly into an electron-positron pair, sharing the transition energy between both particles. Note that pair-production is only possible for transitions with energies greater or equal to 1.022 MeV. The two-photon decay is the third process through which the transition may happen. With the emission of two photons instead of a single photon, the previous angular momentum limitation is no longer an issue, as it is possible to sum $\ell_1 + \ell_2 = 0$ to satisfy the zero angular momentum change between both states.

Although the monopole transition presents no meaningful application for the single real photon decay, this does not mean it is deprived of interest. As previously stated, the electromagnetic transitions is not limited to the single photon decay. Such an example is the correlation between the relation of E0 transitions and the isotope charge radii. From this value of charge radii, one may derive a value for isotope and isomer shifts. Isotope shifts represent the difference in charge radius of neighboring isotopes, while isomer shifts are a description of the charge radius variation between an excited and ground state [8]. Although examination of E0 matrix elements is not a unique method of determining charge radius, as this can be done through electron scattering, it remains an interesting factor to keep in mind.

Putting aside the specific case of observing the two-photon decay in a $0^+ \rightarrow 0^+$ transition, a new issue arises for the study of this exotic decay, where to start looking. A key factor to keep in mind is the expected, daunting, background events created by the single photon emission. At the time of writing this thesis, no clear insight as to where one should look for an 'easier' measurement is available. It is however possible to imagine that, in a scenario where the single photon emission is inhibited by an isotope's structure,

measuring the two-photon decay might be easier.

2.2 Nuclear Shell Model

Similarly to the atomic shell model, which describes the arrangement of electrons in shells around an atom, there is a nuclear shell model for the structure of neutrons and protons within the nucleus. The nuclear shell model uses the Pauli exclusion principle as a base to describe the nucleon (protons and neutrons) structure, that is that no two identical fermions (in this case the nucleons) may occupy the same quantum state simultaneously.

As it is possible to examine the shells for the neutrons and protons within a nucleus independently from each other to determine basic state information, let us for now only discuss the case of protons, understanding fully that the information is also valid for the case of neutrons. If we now consider a three dimensional harmonic oscillator, and observe only the first two levels of a nucleus, we would expect to see a total of 8 protons occupying the first two shell levels. The first level would be comprised of two protons with (n,l,m_l,m_s) values of (0,0,0,$\pm 1/2$), with l being the angular momentum. The second shell would be filled with 6 protons satisfying (1,1,± 1 or 0, $\pm 1/2$).

Similarly to the case of electrons, the outer most protons will be loosely bound to the nucleus. There is however a pairing effect to keep in mind, two protons occupying an outer shell have a smaller change of being ejected than a single, unpaired proton. In order to be considered a pair, two nucleons must be of the same type (proton or neutron), and have opposite spin projections, a concept discussed in the next few line. As such, a nucleus with a full outer shell of protons will have a much higher binding energy than other nuclei with a partially filled outer shell. If we limit our view to this simple model, we could calculate a series of values where one would expect these high binding energies due to full shell, these values are termed magic numbers. Calculating these values returns magic numbers of 2, 8, 20, 40... Experiments have however demonstrated on multiple occasions that these magic numbers are expected to be found at 2, 8, 20, 28, 50... This discrepancy in values is due to the neglected contribution of proton spin, i.e the spin-orbit interaction.

Due to this inclusion of spin-orbit interaction, the energy levels of states of the same

level, but different quantum number j, will no longer be identical. This splitting of states is caused by the alignment of the magnetic moment with respect to the magnetic field. Each nucleon may have their magnetic moment 'aligned' or 'anti-aligned' with the magnetic field. The system in which the nucleon magnetic moment has aligned itself with the nucleus magnetic field will be in a lower energy state than the case where both are anti-aligned.

An extra detail to take into account is the relative angular momentum between each nucleon. At, and close to, the center of the nucleus, this moment will cancel; however this is not the case near the edges of the nucleus. By adding a radial dependence describing this nucleon-nucleon interaction to the shell model, one obtains the spin-orbit coupling term. In addition, one could replace the harmonic oscillator potential, which grows infinitely as the distance from the center increases, by a more realistic potential such as the Woods Saxon potential. This more realistic potential approaches zero as the distance tends to infinity, representative of the short-distance affect of the strong nuclear force.

Combining this shell splitting with the previous, simpler, model one obtains a new series of magic numbers which are 2, 8, 20, 28, 50... which agree with the experimentally determined values. The obtained state positions are not absolute across each nucleus. Certain isotopes, notable deformed nuclei with a highly uneven ratio of protons to neutrons, will have certain states 'swapped' in energy level. These changes will however have no effect on the magic numbers, but will vary the possible transitions for the nucleons in these isotopes.

Similarly to the electron shell model, the position of a given nucleon on a certain shell is not necessarily static; it is possible for a nucleon to 'jump' from one shell to another. Taking for example the first excited state of ^{17}O, there are 4 neutrons in the $1p_{3/2}$ shell as well as 2 neutrons in the $1s_{1/2}$ shell and $1p_{1/2}$shell. A single unpaired neutron will be present in the $2s_{1/2}$ shell. For the purpose of this example, the eight protons are ignored as the completely fill the shells up to $1p_{1/2}$, presenting a stable system on their part. In order to be considered a stable state, the nucleus must find itself in the least energetic configuration, therefore in order to enter a more stable state, this excited Oxygen isotope will have one of it's neutrons drop from the higher $2s_{1/2}$ shell, into the lower energy $1d_{5/2}$

shell. In order to satisfy energy conservation in the system, a photon equal to the energy separating both states would be emitted.

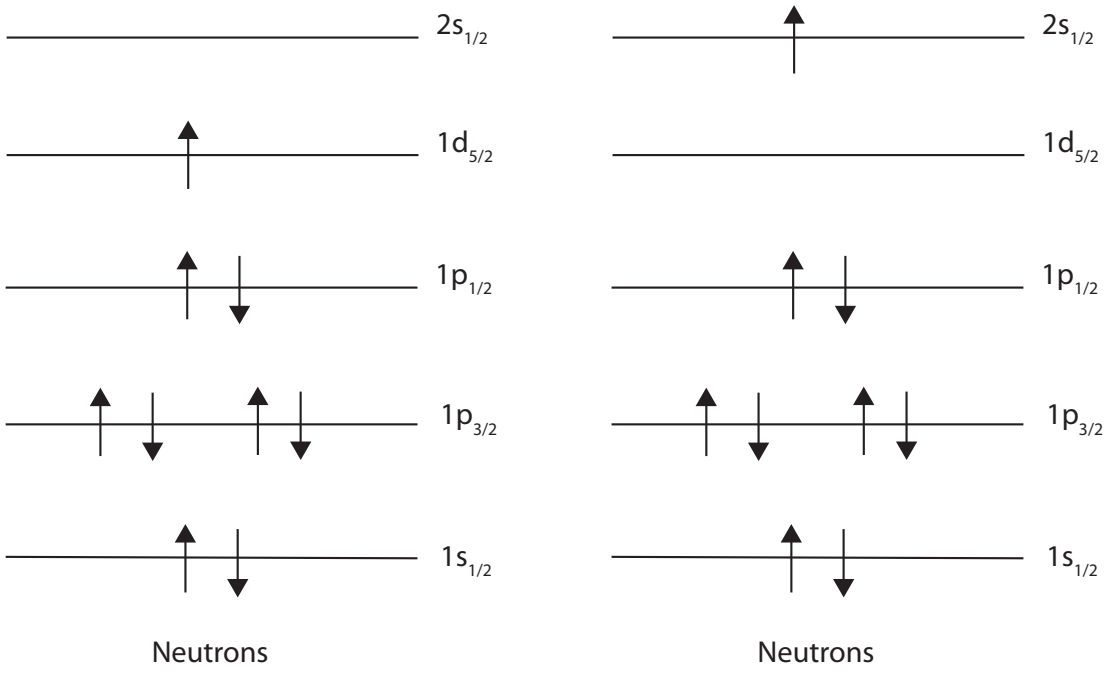

Figure 2.2: Visual representation of the shell model, showing only the neutron configuration, for the ground state (left) and 1st excited state (right) of ^{17}O.

In addition to describing the possible nucleon structure for virtually any isotope, the shell model explains with some success properties of nuclei such as spin and parity of nuclei ground state, as well as their excited state to some extent. Retuning to our example of ^{17}O whose ground state has the $1s_{1/2}$, $1p_{3/2}$, and $1p_{1/2}$ shells filled (for neutrons and protons). This state however has one unpaired neutron in the $1d_{5/2}$ shell, leaving five empty spots, also termed 'holes'. For each nucleon pair, their net angular momentum will be zero. This means that the spin and parity of the state (excited or ground) will be determined by the unpaired nucleon(s), in this case the single unpaired neutron in the $1d_{5/2}$ shell. The spin for this nucleon is easily determined to be $j = 5/2$, and the parity as $\pi = (-1)^l = (-1)^2$. Therefore the ground state of ^{17}O is found to have $j^\pi = \frac{5}{2}^+$. Similarly, spin and parity of the first excited state of ^{17}O is found to be $j^\pi = \frac{1}{2}^+$. A similar analysis can be performed on other isotopes in excited or ground states if the shell model configuration is known.

Although the nuclear shell model does an excellent job at describing the energy state characteristics for lower level states and fairly simple nuclei structure, it falls short as an all-encompassing model. The shell model assumes a symmetrical nuclei when defining the states, therefore any large deformation in the nucleon structure will have a significant impact on the accuracy of the model. This model provides an excellent instrument to understand light nuclei, however as more nucleons come into play, and consequently more shells, the problem becomes too big to be handled by the core nuclear shell model.

Although not directly related to the shell model, the liquid drop model characterizes the nuclei as a liquid, where the molecules (nucleons) are held together only by their nearest neighbors. A strength of this model is the series of interactions it takes into account within the nuclei. The model uses parameters corresponding to the binding of all nucleons within the nucleus by the strong force, electrostatic mutual repulsion from protons, surface energy, asymmetry effects, and pairing effects. This model is unable to explain the presence of magic numbers, nor a few other interesting characteristics; it does however explain the spherical shape of most nuclei and offers a good estimation for atomic masses as well as binding energies.

It was previously stated that the shell model finds a limitation in the shape of nuclei, that is it falls short of correctly modeling highly deformed nuclei. The Nilsson model takes into account the possibly high deformation in nuclei and instead requires a symmetry around an axis [9]. Contrary to the shell model, the single particle orbital angular momentum and total angular momentum are no longer good quantum numbers. For the Nilsson model, only the parity and total angular momentum onto the symmetry axis are good quantum numbers. With these modifications, and later developments in the theory, the model is able to offer model generalization for higher-order deformed and non-deformed nuclei.

Following the shell model predicted behavior, one would expect a very large mean free path for nucleons within the nucleus. This prediction is however not confirmed through particle scattering experiments [10]. The independent-particle model attempts to provide an explanation for this variation between model and experimental observations. The IPM takes the approach that each nucleon moves inside a certain potential well, binding the

nucleon to the nucleus, independently of all other nucleons. In sum, this changes the problem from an N-body problem, to an N single-body problem.

Where the shell model succeeded in accurately describing light atomic nuclei, the interacting boson model is suitable for describing intermediate and heavy atomic nuclei [11]. This model is based on the shell model and on geometrical collective models of the atomic nucleus. The basic assumption of the IBM postulates that the nucleon pairs are represented by bosons with angular momenta $l = 0$ or 2, as opposed to the previous fermion structure. As such the multiple shells appearing in the shell model is reduced to a simpler s-shell ($l = 0$) and d-shell ($l = 2$). A consequence of this model is the difficulty to model Odd nuclei, for which a Bose-Fermi correction must be made.

With this information on the shell model in mind, the question of where best to measure the two-photon decay returns. With the understanding of multipole transition ordering shown through the Weisskopf estimates, and the clear differences in spin values obtained for each state when observing the shell model, it is possible to seek for an ideal case to measure the decay. Within the sea of isotopes presently known and studied, there is a sub-division of certain isotopes, nuclear isomers, with longer half-lives and particular shell structure which might prove interesting in this search. Although there is no clear evidence that nuclear isomers will offer a much cleaner view of the decay, it is possible that their unique characteristics provide a second-to-ideal scenario to measure the two-photon decay.

2.3 Nuclear Isomers

In certain cases the resulting excited state from a nuclear decay, often α or β decay, will be far more stable than the average. These states are termed metastable excited states, and their decay time span the entire range of lifetimes from 10^{15} years (for ^{180m}Ta), to an informal rule of $\sim$1 ns [12]. Nuclei presenting such states, consequently have longer half-lives, and are termed nuclear isomers. Nuclear isomers are characterized by the 'lack' of low level electromagnetic transition routes used in the de-excitation of the isotope. Such states will often have a nuclear spin transition value of several units (i.e proceed through a higher multipole order). As the transition proceeds through higher multipole transitions,

it is evident, from section 2.1, that the isomeric states will have longer half-lives.

Nuclear Isomers are often classified into three classes based on their shape, spin, and spin projection on the axis of symmetry. The three classes are termed fission (or shaped), Spin, and K-isomers [13]. The fission, or shaped, isomers are the result of a transition from an excited state to a lower state with a different shape, they characteristically have superdeformed shapes [14]. K-isomers are present when, during the transition, there is a change in nuclear spin projection along the symmetry axis. Finally there are the Spin isomers, the most common amongst the three types. Spin isomers are the result of having a large spin difference between the initial and final transition states.

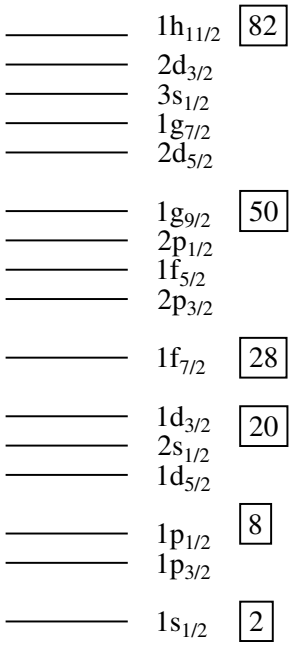

Figure 2.3: Representation of the shell model

One of the great successes of the shell model is the regular appearance of nuclear isomers in the vicinity of closed nucleon shells. The appearance of Isomers is in now way limited to the vicinity of nuclear closed shells, as shown by Patial [13]. Isomers appear over almost the full range of nuclear elements but do seem to cluster around certain areas, that is the shell model's predicted 'magic numbers'. By observing the predicted shell structure near the shell model's magic numbers, one can notice that there is a high spin difference between two nuclear energy states. For example, around the magic number 50, there are the states $1g_{9/2}$ followed by $2p_{1/2}$. Noting a spin difference between both states of 4 units, one can determine that a nucleon transition between these two states would have to proceed through an hexadecapole transition at minimum. A similar observation can be made close to the magic numbers 82 and 28.

An isomer commonly used in medical physics is ^{99m}Tc with a half-life of $\sim$6 hours. With 56 neutrons and 43 protons, this isotope has protons in the $1g_{9/2}$ shell, left only to transition to the $2p_{1/2}$ shell. As well, the commonly used ^{137m}Ba isomer with a half-life of $\sim$ 2.5 mins, has 81 neutrons and 56 protons; placing a neutron hole in the $1h_{11/2}$ shell.

The de-excitation process will yield a transition between spins 11/2 and 3/2. It is also worth noting that the even though there is a greater spin change for the Ba isomer than the Tc, the half-life for the Ba isomer is shorter than that of Tc. This is due to the half-life's dependence on spin difference as well as excitation energy, as previously shown in Table 2.1.

2.4 Second Order Photon Emission

In the case of the second order photon emission, physically represented as a two-photon emission for which both photons' sum energy is equal to that of the first order single photon. Referring back to Figure 2.1, diagrams (b) and (c) represent the same two-photon decay through an intermediate state $|n\rangle$. The presence of two diagrams (b) and (c) is to demonstrate that both emitted photons can be interchanged between vertices. The third decay option is a two-photon decay of first order, shown in digram (d), referred to as the seagull contribution.

The seagull contribution arises through the seagull operator within the interaction Hamiltonian between a nucleus and an electromagnetic radiation field. This Hamiltonian can be described by [15]

$$H_{int} = \int j_\mu(x) A^\mu d^3x + \frac{1}{2} \int B_{\mu\nu}(x,y) A^\mu(x) A^\nu(y) d^3x d^3y \tag{2.6}$$

with the current operator $j_\mu(x) = (\rho(\mathbf{x}), \mathbf{j}(\mathbf{x}))$ and the seagull operator $\mathbf{B}^{\mu\nu}(\mathbf{x}, \mathbf{y})$. This seagull operator is a result from the non-relativistic approximation of the nucleus. In a fully relativistic theory, the seagull operator corresponds to a sum over very high mass states, containing virtual nucleon-antinucleon pairs excitations and de-excitations. Allowing for the principle of the Heisenberg uncertainty principle, these increasingly reduced contributions of the higher mass states are represented by this operator. This seagull operator term is however only necessary if both photon transitions are magnetic transitions.

Neglecting the second term in Equation 2.6, and treating the problem in first order perturbation theory, yields single photon decay equation (see diagram (a) in Figure 2.1).

2.5 History of the Two-Photon Decay

In 1930, Maria Göppert-Mayer made the first investigation into the two photon decay in her doctoral thesis where she examined the two light quanta absorption and emission [3]. In this exotic, second order process, an excited state decays via a higher lying intermediate virtual state to a lower lying state, emitting two photons in coincidence. Such an event is represented in a diagram drawn in Maria Göppert-Mayer's thesis, see Figure 2.4. The sum energy of these two photons is equal to the transition energy from the excited state to the initial state. It is interesting to note that the two-photon decay probability involves a sum over all states (n') of the atom, as opposed to a single, constant n' state. This particular characteristic makes the study of the two-photon of particular interest due to this unique observable value which depends on the entire structure of the system examined.

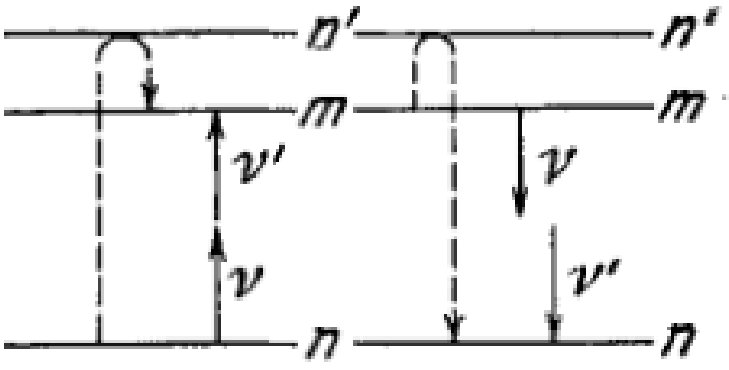

Figure 2.4: The two-photon absorption and emission process(taken from [3]). On the left is the representation of the two light quanta absorption. On the right is the two light quanta emission (two-photon decay).

Kramp demonstrated in his 1987 paper [6] that the branching ratio for the two-photon decay can be directly linked to the diagonal magnetic susceptibility (χ_P), which is proportional to the sum over all B(E1)-values and B(M1)-values. In order to determine this quantitie, a measurement of the electric and magnetic dipole responses over the full energy range is required. Doing so is experimentally challenging, and is mainly accomplished through zero degree proton scattering [16].

According to Kramp, the magnetic dipole transition susceptibility can be written as

$$\chi^{12} = \chi_P^{12} + \chi_D^{12} \tag{2.7}$$

where χ_P^{12} is defined as the paramagnetic transition susceptibility and χ_D^{12} is the diamagnetic transition susceptibility. This paramagnetic transition susceptibility is closely related to the paramagnetic susceptibility of the ground state (χ_P) given in Equation 2.8. Similarly, the diagonal electric dipole polarizability (α_{E1}) is shown in Equation 2.8 [6].

$$\begin{aligned} \chi_P &= \frac{4}{9}\pi \cdot 2 \sum_n \frac{|\left\langle 0_1^+ \right| |M(M1)| \, |1_n^-\rangle \, |^2}{E_n} \\ \alpha_{E1} &= \frac{4}{9}\pi \cdot 2 \sum_n \frac{|\left\langle 0_1^+ \right| |iM(E1)| \, |1_n^-\rangle \, |^2}{E_n} \end{aligned} \tag{2.8}$$

The diagonal electric dipole polarizability has so far shown to be of interest in the domain of nuclear physics. Recent papers have used it to restrict the parameters of the equation of state [17], and to determine the neutron skin thickness [18]. In both these examples the diagonal electric dipole polarizability factor was determined through an alternate method, however one might expect the factor obtained through analysis of the two-photon decay to be usable for the same end goals. The possibility of this still requires a detailed theoretical investigation of the problem.

In 1987, J. Kramp published the results of his experiment on the two-photon decay in the specific case of $0^+ \rightarrow 0^+$ transitions, observed in the ^{16}O, ^{90}Zr, and ^{40}Ca isotopes [6]. These particular isotopes, where the single photon emission is forbidden by angular momentum conservation, prove to be ideal candidates to observe the two-photon decay without the interference of the single photon emission (refer back to section 2.1).

There have been previous reported attempts to measure the two-photon decay in cases other than the $0^+ \rightarrow 0^+$ transition. There has however so far been no report of an experiment which has managed to accurately measure the branching ratio for the two-photon decay. An experiment led by M. Music has however determined an upper limit for the branching ratio of $\Gamma_{\gamma\gamma}/\Gamma_{tot} < 10^{-5}$ for the 2^+ excited state of ^{16}O [19].

In 2011, D.J. Millener made a presentation on the 2-gamma decay of the 662-keV 11/2 isomer of ^{137}Ba at the American Physical Society [20]. The two-photon decay branching

ratio for a ^{137}Cs radioactive source was examined in his experiment. From Millener's experiment and derivations, a preliminary value of 2.06×10^{-6} is obtained for the 2-gamma/1-gamma intensity ratio [20]. This specific experiment was however unable to experimentally confirm an accurate value due to the limitations of the used NaI detectors. The experiment did however reveal a peak profile for the two-photon decay.

2.6 The Case of ^{137}Ba

Below we consider the theoretical aspects and components of using ^{137}Ba as a source for investigating the two-photon decay. The results and concepts demonstrated in this following section are based on the work performed by D.J. Millener (in Ref. [21]) who developed a simple nuclear structure model and thereafter calculated the relevant two-photon decay observables.

The 662keV transition from the radioactive ^{137}Ba proceeds via an M4-transition from the excited $1h_{11/2}{}^{-}$ state to the $2d_{3/2}{}^{+}$ ground state. As the two-photon decay proceeds via higher-lying intermediate states, it is possible to use the spin selection rule to determine the allowed values for the total angular momentum transfer (J).

$$\begin{aligned} |I_i - I_f| \leq J \leq |I_i + I_f|, \\ |L' - L| \leq J \leq |L' + L|, \end{aligned} \tag{2.9}$$

From these, it is possible to obtain values of J=4, 5, 6, 7. With a very good approximation, the sum can be limited to J=4 [22], thus the study can be limited to the case where the multipolarities L, L' sum to J=4 (L+L'=4). Therefore, the considered transitions for this particular decay are E1+M3, M1+E3, and E2+M2. There is of course the need to confirm that contributions such as E2+E3 are truly negligible. Due to the constraints of the previous approximations, the allowed intermediate states will have angular momentum values of j=5/2, 7/2, or 9/2.

For the case of ^{137}Ba with its 56 protons and 81 neutrons, the single particle state

equation for the neutrons is written as

$$\begin{gathered}\text{Protons} : [50](1g_{7/2})^6 \\ \text{Neutrons} : [50](1g_{7/2})^8(2d_{5/2})^6(3s_{1/2})^2(1h_{11/2})^{11}(2d_{3/2})^4\end{gathered} \tag{2.10}$$

This particle state equation is determined through experimental measurements. Although this varies slightly from the standard shell positioning offered through the nuclear shell model, the same concepts from the shell model still apply.

In order to satisfy the angular momentum values determined earlier, it is important to understand what happens with the neutron hole left in the $1h_{11/2}$ orbital. In order to obtain j=5/2 the neutron hole would fall in the $2d_{5/2}$ orbital, for j=7/2 the hole would fall in the $1g_{7/2}$, finally the j=9/2 would have the neutron hole in the $1g_{9/2}$ orbital. Note that a transition to the, for example $2f_{7/2}$ orbital is not possible since there is no one-step de-excitation back to the ground state

Making use of the selection rules for Electromagnetic Transitions, the transition pairs can be associated to the neutron hole transitions described above. The transition from $1h_{11/2}$ to $2d_{5/2}$ and finishing at $2d_{3/2}$ will proceed through the E3+M1 transitions. The other two transitions mentioned above are also represented in Figure 2.5.

It is also important to understand that transitions to higher orbitals of the same spin, such as $1h_{9/2}$, $2f_{5/2}$, or $1i_{11/2}$, are ignored in this simple model. This is in most part due to the inverse dependence on energy square for the two-photon probability [1].

It is now evident that the two-photon decay will proceed via one of two methods, either through a quadrupole-quadrupole transition, or a dipole-octupole transition. Given this, it becomes immediately interesting to know which transition will be the primary source for the two-photon decay, as well as understanding the branching ratio specific to either transition methods.

Although it is theoretically possible to distinguish both multipole pairs through their angular dependence, this would prove experimentally challenging. In order to adequately determine the angular dependence, the detector positioning with respect to each other would need to be evaluated to great precision. In addition, there would need to be a various set of angles for different detector pairs; creating a very complex experimental setup. An

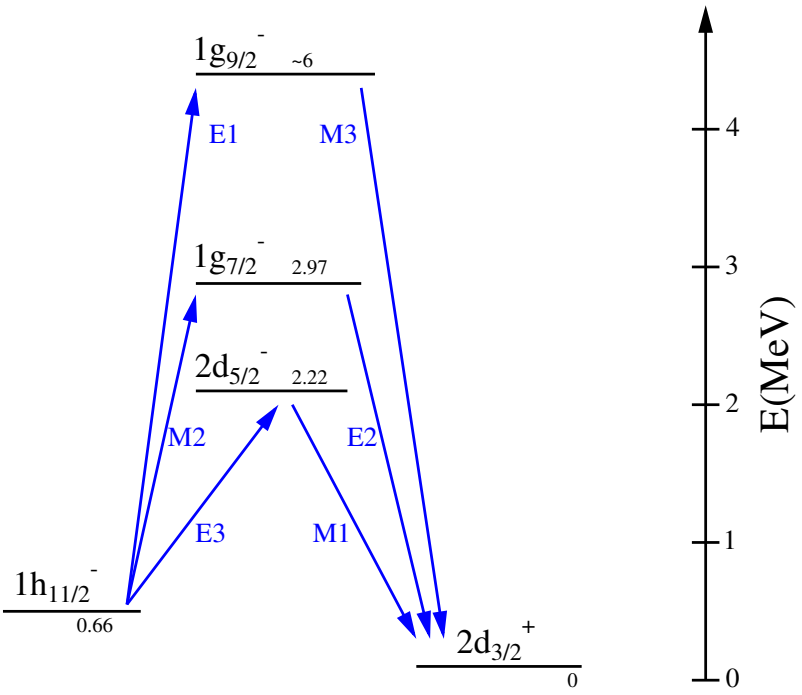

Figure 2.5: Model representation of transitions for select cases of J=4, allowing for the two-photon decay.

alternate method to separate both multipole pairs is to determine the dependence of the branching ratio on the detected photon energy. Measuring an accurate energy distribution should allow for a clear separation of both multipole pairs.

In addition to separating both multipole pairs, the accurate measuring of photon energy distribution allows for a much clearer distinction between the two-photon event and other interfering events; notably Compton scattering.

Calculations performed by Millener using the IPM, returned the two-photon branching ratio values for E2+M2 ($1.28{\cdot}10^{-6}$), and M1+E3 ($0.78{\cdot}10^{-6}$). The full value for the branching ratio was determined to be $2.06{\cdot}10^{-6}$. Note that the contribution from the E1+M3 transition is ignored as the contribution from E1 matrix elements are negligibly small [22].

From Kramp's study, one can obtain the differential two-photon decay probability for a transition from a state with spin I_i to a final spin I_f after integrating over all angles [22].

$$\begin{aligned}\frac{d^2\Gamma_{\gamma\gamma}}{d\omega d(\cos\theta)} =& \frac{\omega\omega'}{(2I_i+1)\pi}\cdot \sum_{LL'SS'\bar{L}\bar{L}'\bar{S}\bar{S}'KJ}\sum_{\lambda\lambda'} \\ & \{\lambda^{S+\bar{S}}\lambda'^{S'+\bar{S}'}\frac{\hat{J}^2}{L\hat{\bar{L}}'}(-)^{\lambda+\lambda'+L'+\bar{L}}(-)^{L'+\bar{L}'+K} \\ & \cdot\left\langle L-\lambda\bar{L}\lambda\,\middle|\,K0\right\rangle\cdot\left\langle L'-\lambda'\bar{L}'\lambda'\,\middle|\,K0\right\rangle\cdot U(\bar{L}JKL',\bar{L}'L) \\ & \cdot P_K(\cos\theta)\cdot P_J(S'L'SL,\omega'\omega)\cdot P_J(\bar{S}'\bar{L}'\bar{S}\bar{L},\omega'\omega)\}\end{aligned} \tag{2.11}$$

In this case, S, S', $\bar{S}$, and $\bar{S}'$ represent the electromagnetic multipoles, with S=0 for electric, and S=1 for magnetic. λ represents the photon helicity, thus is limited to $\lambda = \pm 1$, and $U(\bar{L}JKL',\bar{L}'L)$ is related to the Clebsch-gordan coefficients and the 6j symbol.

After integrating Equation 2.11 over d$(\cos\theta)$, considering only the E2+M2 and M1+E3 multipole pairs, and with the denominator assumed to be independent of energy ω, one obtains

$$\frac{d\Gamma_{\gamma\gamma}}{d\omega}\sim\frac{\langle I_f|\,|i^{L'-S'}M(S'L')|\,|I_n\rangle^2\left\langle I_n\,\middle\|\,i^{L-S}M(SL)\,\middle\|\,I_n\right\rangle^2}{\Delta E^2}\left[\omega^{2L+1}\omega'^{2L'+1}+\omega^{2L'+1}\omega'^{2L+1}\right]. \tag{2.12}$$

From the Legendre polynomial $\mathrm{P_K}$ in Equation 2.11 one can obtain the angular distribution of each contributing multipole pair. For the quadrupole-quadrupole pair, the angular distribution is given as

$$W(\theta)=1+\tfrac{1}{3}P_1(\cos\theta)+\tfrac{5}{49}P_2(\cos\theta)+\tfrac{1}{7}P_3(\cos\theta)+\tfrac{40}{441}P_4(\cos\theta), \tag{2.13}$$

while for the dipole-octupole pair, the angular distribution is given by

$$W(\theta)=1-\tfrac{1}{8}P_2(\cos\theta)+\tfrac{3}{8}P_3(\cos\theta). \tag{2.14}$$

Furthermore, each multipole transition will demonstrate a dependence of $\Gamma_{\gamma\gamma}/d\omega$ on the photon energy ω. As demonstrated in Equation 2.12 one obtains, $\Gamma_{\gamma\gamma}/d\omega\sim\omega^5\omega'^5$ for the case of a quadrupole-quadrupole transition, and $\Gamma_{\gamma\gamma}/d\omega\sim\omega^3\omega'^7+\omega^7\omega'^3$ for the case of a dipole-octupole transition. In addition to the pre-existing condition for the ^{137}Ba

transition where $\omega + \omega' = 662$ keV is necessary. Using these conditions it is possible to demonstrate the general shape of this energy distribution for both quadrupole-quadrupole and dipole-octupole (left plot in Figure 2.6). From the energy distribution shown, it is evident that the quadrupole-quadrupole transition favors and equal energy distribution of $\omega_1 = \omega_2 = 331$ keV, while the dipole-octupole transition favors $\omega_1 \simeq 231$ keV and $\omega_2 \simeq 471$ keV.

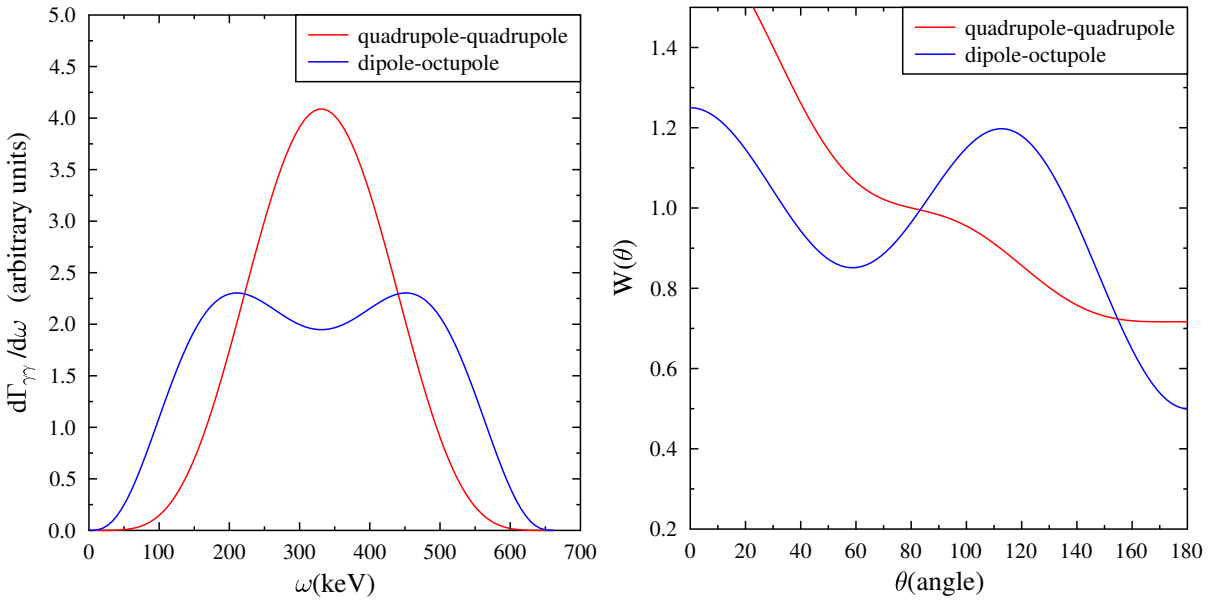

Figure 2.6: The two-photon dependence on photon energy ω (left figure) and relative angle between both emitted photons (right figure). Each distribution is shown for both multipole pairs: quadrupole-quadrupole (red) and dipole-octupole (blue). Note that both plots in the left figure were normalized to have identical areas for a better visual representation.

Two energy gates were applied to the multipole energy distribution represented by $0 < |E1 - E2| < 250$ and $250 < |E1 - E2| < 450$. These conditions represent an energy gate around the central peak (between 206 keV and 456 keV), and on the edges of the dipole-octupole peaks (between 106 keV and 206 keV, and between 456 keV and 556 keV. One can integrate both multipole functions over both energy gates. From there a ratio of the center energy gate to the edge energy gates can be taken for both multipole functions.

The values for the energy gates were selected such that the the difference between both ratios was a great as possible in order to simplify differentiation between both multipole pairs.

The purpose of determining these theoretical ratios is to create a basis to which the experimental ratios may be compared to once obtained. Ideally, once similar energy gates are applied to the obtained energy spectra, an almost ideal ratio value would be found; or at the very least a similar value. Such a similar value would allow the determination of which multipole transition is the most dominant on this two-photon decay process.

The experimental advantages for the use of a ^{137}Cs radioactive source is discussed later in section 3.4.

Chapter 3

Experiment

It has been previously outlined that the two-photon decay is an exotic decay, and in the case where the single photon decay is allowed, one has to deal with many more experimental complications. As the two-photon decay occurs, in this particular case, on the order of a few times per day, it is crucial to develop an ideal experimental setup. In addition to this, it is important to investigate the background radiation consistently present in the vicinity of the experimental apparatus.

The first step towards detecting the two-photon decay is to select detectors with high time and energy resolution. In recent years, $LaBr_3$ crystals have been developed for the use of scintillation detectors, showing highly improved timing and energy resolutions compared to previous scintillation crystals (see Figure 3.1). This experiment made use of multiple $LaBr_3$ 3x3 inch scintillation detectors. The typical energy resolution of these crystals at 662 keV is of 3%, compared to 7% with NaI detectors [23]. Both the NaI and BGO crystals have been used as scintillation detector crystals over the past few years. $LaBr_3$ crystals offer a new alternative with very high stopping power due to the high Z value of Lanthanum and Bromide.

In addition to these detectors, plastic scintillators where used in order to act as active shielding for the experimental setup. The plastic scintillators were positioned on top of the experimental setup in order to serve as veto to a random $LaBr_3$ coincidence. That is if one plastic scintillator detects an event at the same moment as two $LaBr_3$ crystals (or more) detect a coincidence event, the coincident event is disregarded for further analysis. Observing the effect of these plastic scintillators on the energy window from 652 to 672 keV, the number of events per day and detector pair was reduced by a factor of $\sim$1.5.

Although the timing resolution of $LaBr_3$ crystals has been shown to be excellent, this

is not fast enough to separate direct Compton scattering events and two-photons events. As such it is important to build an experimental setup which will suppress these unwanted direct Compton scattering events.

Parameter:	ρ	MP	X_0^*	R_M^*	dE^*/dx	λ_I^*	τ_{decay}	λ_{max}	$n^\natural$	Relative output†	Hygro-scopic?	$d(\text{LY})/dT$
Units:	g/cm^3	°C	cm	cm	MeV/cm	cm	ns	nm				%/°C‡
NaI(Tl)	3.67	651	2.59	4.13	4.8	42.9	230	410	1.85	100	yes	−0.2
BGO	7.13	1050	1.12	2.23	9.0	22.8	300	480	2.15	21	no	−0.9
BaF_2	4.89	1280	2.03	3.10	6.5	30.7	630^s	300^s	1.50	36^s	no	−1.3^s
							0.9^f	220^f		3.4^f		∼0^f
CsI(Tl)	4.51	621	1.86	3.57	5.6	39.3	1300	560	1.79	165	slight	0.3
CsI(pure)	4.51	621	1.86	3.57	5.6	39.3	35^s	420^s	1.95	3.6^s	slight	−1.3
							6^f	310^f		1.1^f		
$PbWO_4$	8.3	1123	0.89	2.00	10.1	20.7	30^s	425^s	2.20	0.083^s	no	−2.7
							10^f	420^f		0.29^f		
LSO(Ce)	7.40	2050	1.14	2.07	9.6	20.9	40	402	1.82	83	no	−0.2
$LaBr_3$(Ce)	5.29	788	1.88	2.85	6.9	30.4	20	356	1.9	130	yes	0.2

* Numerical values calculated using formulae in this review.
$^\natural$ Refractive index at the wavelength of the emission maximum.
† Relative light output measured for samples of 1.5 X_0 cube with a Tyvek paper wrapping and a full end face coupled to a photodetector. The quantum efficiencies of the photodetector is taken out.
‡ Variation of light yield with temperature evaluated at the room temperature.
f = fast component, s = slow component

Figure 3.1: Parameter table for scintillation detector crystals [4]

The utilized radioactive sources for this experiment were two ^{60}Co sources of ∼170 kBq and 69.4 MBq for early testing and experimental development, as well as a ^{137}Cs source with a strength of $487{\cdot}10^3$ 662 kev-photons per seconds for the true two-photon experiment. In order to limit the amount of Compton events in the experimental setup, the source holder was made from simple cardboard. Such a material would appear as almost transparent to the emitted photons, resulting in virtually no second order 'sequential' Compton scattering events.

3.1 Physics Constraints

It has already been made clear that the two-photon decay is a second order, exotic decay for any nucleus. In the case where the single photon decay is allowed, it can be seen that measuring this branching ratio will be a difficult task. In order to isolate the two-photon event from other measured events, it is important to first understand the effects which will interfere with the measurements, as well as the two types of coincidences which will be used in this experiment: Timing and energy coincidences.

An event in timing coincidence is defined, within the confines of this experiment, as two detectors measuring separate events within a predefined time window. In most cases both events in timing coincidence will have a seemingly random energy distribution, or more specifically, will not be of the energies the experiment calls for. In this experiment, a known sum energy is required between both events. Should two events satisfy this sum energy condition, they would be classified as being in energy coincidence. In order to properly select the desired events within the sea of other events, it is crucial to ensure both the timing coincidence and energy coincidence criteria are satisfied.

In such a coincidence experiment, there are two basic difficulties which make the observation of the two-photon decay difficult. The very low branching ratio described previously on the order of 10^{-6}, and secondly the numerous other coincidence events observed which do not represent the two-photon decay. In order to separate these "accidental" coincidence events from the true two-photon decay events, it is crucial to understand these events and their exact effects.

Compton Scattering

As the branching ration in ^{137}Ba is predicted to be $2.06 \cdot 10^{-6}$ [20], the single photon decay is about six orders of magnitude more likely than the two-photon decay. As such the first issue to consider is that of Compton scattering of the 662 keV photon.

The 'direct' Compton scattering occurs when the initial photon deposits part of its energy into one detector and then proceeds to deposit the rest of its energy in a second detector. The sum energy of this event would thus be equal to the initial photon energy

and would occur within a very short time frame, making these events very difficult to separate from two-photon events.

It will thus be necessary to create an experimental setup which removes these events from detection. The evident solution is to make use of lead shielding, due to its high density and Z value, between detectors in order to absorb the scattered photons.

A lead shielding width of 7.5 cm was selected to be placed between each detector in order to absorb the totality of the Compton scattered photons (see section 3.2). Care was also taken to insure no open slits were left between the lead bricks.

The second significant issue arises from 'sequential' Compton scattering, which occurs when an initial photon scatters from a detector at $\sim$180°, scattering again against an object near the source, or the source itself, into a second detector. Contrary to to the 'direct' Compton scattering, this event would be unaffected by the lead shielding, however would be distinguishable from the two-photon event through energy and time analysis.

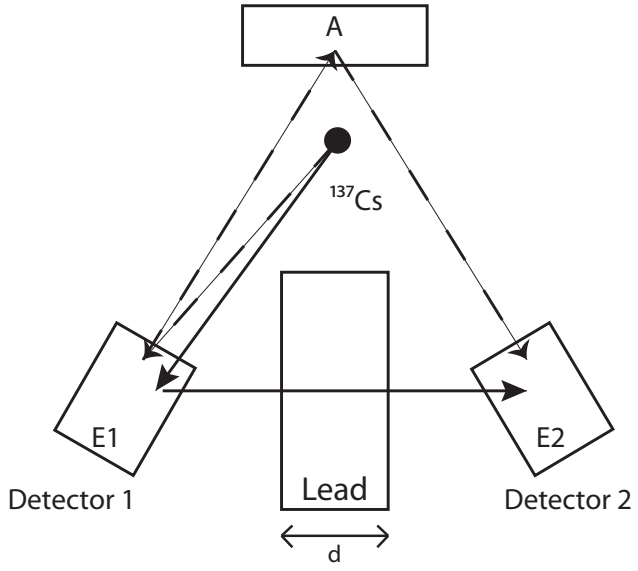

Figure 3.2: Direct Compton scattering is represented by a gamma-ray depositing energy E1 into detector 1, and scattering into detector 2 (solid black arrows). The doted black arrows represent the 'sequential' Compton scattering where the initial photon deposits energy in detector 1, reflects back by $\sim$180° and is scattered again on material 'A' into detector 2.

By taking the Compton scattering formula

$$E'_\gamma = \frac{E_\gamma}{1 + \frac{E_\gamma}{m_e c^2}(1 - cos\theta)}, \tag{3.1}$$

it can be easily determined that the photon scattered at 180° for a 662 keV photon, would have an energy of ∼184 keV. After being scattered by say ∼72° by a material 'A' (see Figure 3.2) into a second detector, it would then have an energy of ∼125 keV. The sum energy between both detectors would be 478 keV + 125 keV = 603 keV. This peak would thus be defined enough with respect to the two-photon peak to easily tell the two apart, the issue arises from the strength of this peak. Due to the high difference in event rate, the 'sequential' Compton scattering peak would make the determination and analysis of the two-photon peak very difficult.

A simulation of 2 detectors at 72° with 10^9 events emitted from the source was done with enough lead to suppress all direct Compton scattering in order to observe the result of sequential Compton scattering. The resulting sum energy spectrum is shown in Figure 3.3.

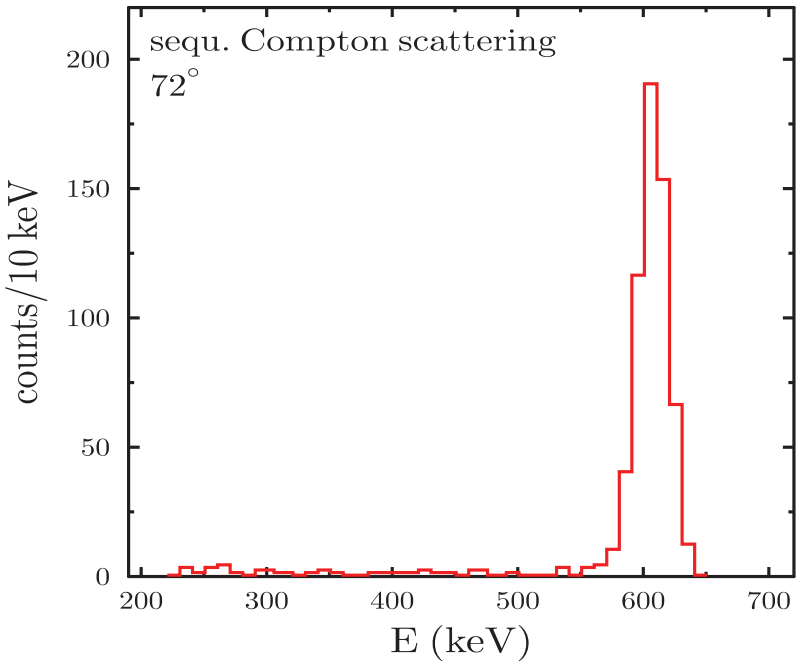

Figure 3.3: Sum energy spectrum for both detectors involved in the 'sequential' Compton scattering for a GEANT4 simulation of two detectors at 72° from each other, and 22cm away from the source, with 10^9 events. Image taken from [1].

In order to remove this effect, it is possible to add an energy gate around 478 keV and 125 keV which would veto the event, discarding it from further analysis. The use of time gates are also considered due to the extra travel time. In the case of 72° detector setup, both detectors are placed at 22.5 cm from the source, making the sequentially scattered photons travel a total path of ∼45 cm. That is the timing difference peak would be offset by ∼1.5 ns from center. This shift however is not enough to offer a clear separation between both peaks.

Cosmic Rays

With the constant barrage of high energy cosmic rays, it is natural to expect them to interact with the experimental setup, even confined to a lead castle. Cosmic rays may create a coincidence event in a few methods. (1) A cosmic ray (muon) may travel through two detector crystals, ionizing the electrons and triggering a coincidence event. Placing plastic scintillators above the experimental setup will offer a veto to most of these events. (2) A cosmic ray may interact with the lead castle (or other surrounding structure) and create a photon shower, which will in turn trigger a coincidence event if two, or more, of these photons reach two detectors.

Pair Annihilation

Though not relevant to the current experiment, pair annihilation is a process which occurs when a subatomic particle collides with its respective antiparticle. Due to energy and momentum conservation the two particles will be transformed, for low energies, into two photons emitted in opposite directions. In this case, electron-positron annihilation will be the only case examined. With an annihilation occurring within a nucleus, both emitted photons will have energy values of 511 keV. Due to this energy restriction, it is important to note that this process may only occur if the gamma-ray has an energy equal or greater than 1.022 MeV.

Such a decay could easily cause a timing coincidence event and potentially an energy coincidence event. As both photons would be emitted at the same time, and in opposite directions, they could potentially arrive into separate detectors at the same moment.

Although the sum energies from both photons would most likely not sum up to a transition energy, it could be part of a random sum which would coincide with a transition energy.

Other Random Coincidences

If two atoms from the source decay at the same moment, and the resulting photons interact with separate detector crystals, a coincidence event will be recorded. This type of coincidence should also be considered in the case where an isotope emits multiple cascade gammas as it decays. In such a case, it is possible for two or more photons to reach the detectors and cause both an energy and timing coincidence event.

Since the detector crystals are radioactive by nature, it is a common occurrence for the crystals themselves to emit a photon which will then trigger and event within the detector. This particular process is known as internal radioactivity. If such an event occurs at the same moment another photon enters a separate detector, this would cause a timing coincidence event, and possibly an energy coincidence event.

As a portion of the experiment is being performed in a basement laboratory, the possibility of an excited γ-ray originating from ground radioactivity interacting with the detector crystals, needs to be considered. If, such as in the case of internal radioactivity, the photon from ground radioactivity interacts with a detector crystal at the same moment a photon originating from the source interacts with another detector, a coincidence event will be recorded.

3.2 γ-Ray Attenuation Through Lead

The first step to perform these experiments was to determine the width of lead shielding necessary between two detectors in order to suppress Compton scattering events. The attenuation measurements were performed for the 1332 keV and 1173 keV energy lines.

Triple Detector setup

The first setup for the Compton scattering suppression is shown in Figure 3.4. Three $LaBr_3$ scintillation detectors were positioned around a 49.4 MBq ^{60}Co source. Detector 1

and 2 were placed 22 cm away from the source while detector 3 was placed at 15 cm from the source. Detectors 1 and 2 (see figure) were placed at 90° from each other.

The varying lead shield was placed between detector 1 and 2, where the shield could vary in width from 0 cm to 17.5 cm. This width is limited by the geometry of the experimental setup.

This setup was built in order to observe the absorption effect of the Compton scattered photons from detector 1 to detector 2 (or vice-versa). In order to obtain a cleaner result, a 10 cm lead shield was later added between the source and detector 2. This causes the photons scattering off detector 1 to be much more predominant than the much fewer scattering off of detector 2.

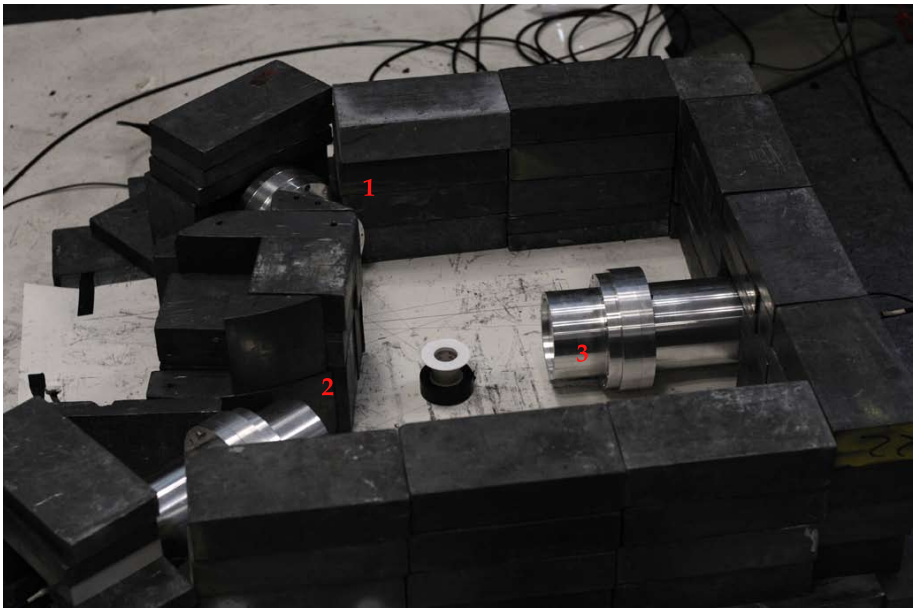

Figure 3.4: Three $LaBr_3$ detector setup (source and lid missing). Note that for the experiment a steel and lead "lid" was placed atop the setup to reduce outgoing radiation.

In order to properly measure the Compton scattering events, an energy gate was placed on detector three around 1332 keV (1173 keV). A second energy gate was then placed where the sum energy of detectors 1 and 2 must be 1173 keV (1332 keV). Both of these energy conditions must be satisfied at the same time for the event to be considered. Since the intermediate state has a lifetime of 0.9 ps, it is possible to apply this timing coincidence logic to the experimental setup.

In order to properly understand what is displayed in Figure 3.5 and Figure 3.6, it is important to understand that the images display the energy captured in detector 1 versus the energy captured in detector 2. In addition, there are conditions placed for timing coincidence between both detectors, such that only the events in timing coincidence between detector 1 and 2 will be used.

In Figure 3.5 it is shown that the majority of the examined photons deposit either ∼1170 keV or ∼900 keV (for photons of an original energy of 1332.5 keV and 1173.2 keV respectively) in detector 1 and then deposit their remaining energy into detector 2. The extended diagonal line of these Compton scattered events indicates the variation in deposited energy in each detector.

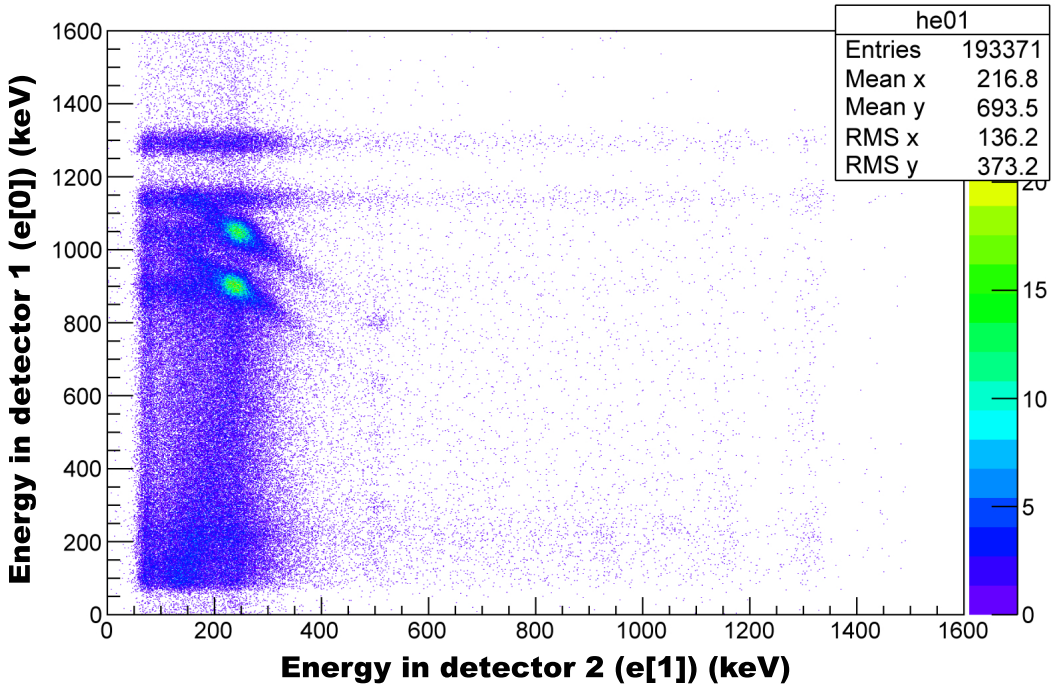

Figure 3.5: E1 versus E2 with timing conditions and no Compton scattering lead shielding

In addition to this, it is possible to see the single and double escape of pair production from the 1332.5 keV photon. Along the 511 keV energy detected in detector 2, energies are shown at ∼821 keV and ∼310 keV in detector 1. As well, the single escape is observed for the 1173.2 keV γ-ray is observed at e[1]=511 keV and e[0]$\simeq$622 keV. These single

and double escapes represent the cases where, when pair-production occurs, one or two of the annihilation photons escape detector 1. One of these photons is required, by the experimental coincidence logic, to have reached detector 2; the second one may either be capture by detector 1 (single escape) or escape detector 1 (double escape).

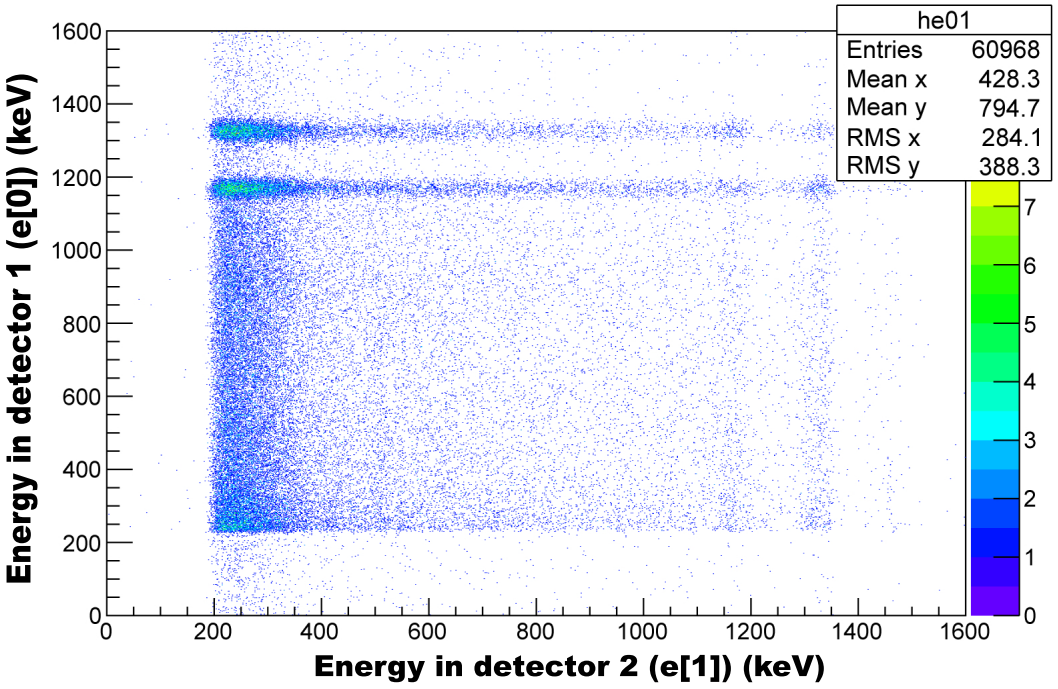

Figure 3.6: E1 versus E2 with timing conditions and 2.5cm lead shielding

Following the observations made in Figure 3.5 and Figure 3.6 where it can be seen that only a minute fraction, if any, of the Compton scattered gamma-rays cross the smallest lead interval (2.5 cm) in a period of ∼45 minutes. From Figure 3.5 it can be seen that the Compton scattered photon energies are centered around 250-300 keV. Although this allows for the examination of lead absorption for low energies, the process would time consuming. In order to observe a greater range of gamma-ray absorption by lead, the second setup (two detectors) was implemented in order to observe the 1332.5 keV and 1173.2 keV absorptions through lead (Figure 3.7).

Using NIST absorption coefficients for lead; it is possible to determine the theoretical value for 2.5 cm of lead, using the absorption equation $A(x) = A(0)\exp((\mu/\rho)\cdot\rho\cdot x)$, where the value of μ/ρ is obtained from the official NIST website [24], and $A(0)$ is taken

to be $A(0) = 1$.

$$\begin{aligned} A(x) &= 1 * \exp(-0.4\text{cm}^2/\text{g} \cdot 11.349\text{g/cm}^3 \cdot x) \\ A(2.5) &= \exp(-11.349) \\ A(2.5) &= 0.000012 \end{aligned} \tag{3.2}$$

The results from both Figure 3.6 and Equation 3.2 demonstrate the need to either perform this experiment with very long measurement times, or observe the absorptions of higher energy photons. Thus, the absorption of 1173.2 keV and 1332.5 keV was determined to be the next viable step for this experiment.

Although the triple detector setup with varying lead shield width was not useful in determining lead absorption of Compton scattered photons; the information gathered by the triple coincidence run does provide interesting information. The most interesting feature being the cluster of points around e[1] equal to ∼250 keV (the energy deposited in detector 2) in Figure 3.5. This cluster of points explicitly shows the Compton scattered photons' energy distribution.

With the lead shielding placed between the source and detector 2, most events triggered when e[0] is 1332.5 keV or 1173.2 keV are low energy level random events, most often below 400 keV. There are however cases where either of the 1332.5 keV or 1173.2 keV are in coincidence with other 1332.5 keV or 1173.2 keV photons. These types of coincidences are indicative of when two atoms within the same radioactive sample decay at the same time, and their respective emitted photons are captured by the two detectors.

Double Detector setup

The double detector setup had two detectors placed in line with the ^{60}Co radioactive source. Detector 2 was placed at 25 cm from the source while detector 1 was placed at 15 cm from the source. The varying lead shield was placed between detector 2 and the source. Contrary to the previous setup, where the absorption of the Compton scattered photons was observed, the two detector setup was built to analyze the absorption of both the 1332.5 keV and 1173.2 keV photons through lead from a 49.4 MBq ^{60}Co source as oppose to the scattered gamma-rays done in the three detector setup.

With the two detector setup, the absorption of the 1332.5 keV and 1773.2 keV γ-rays

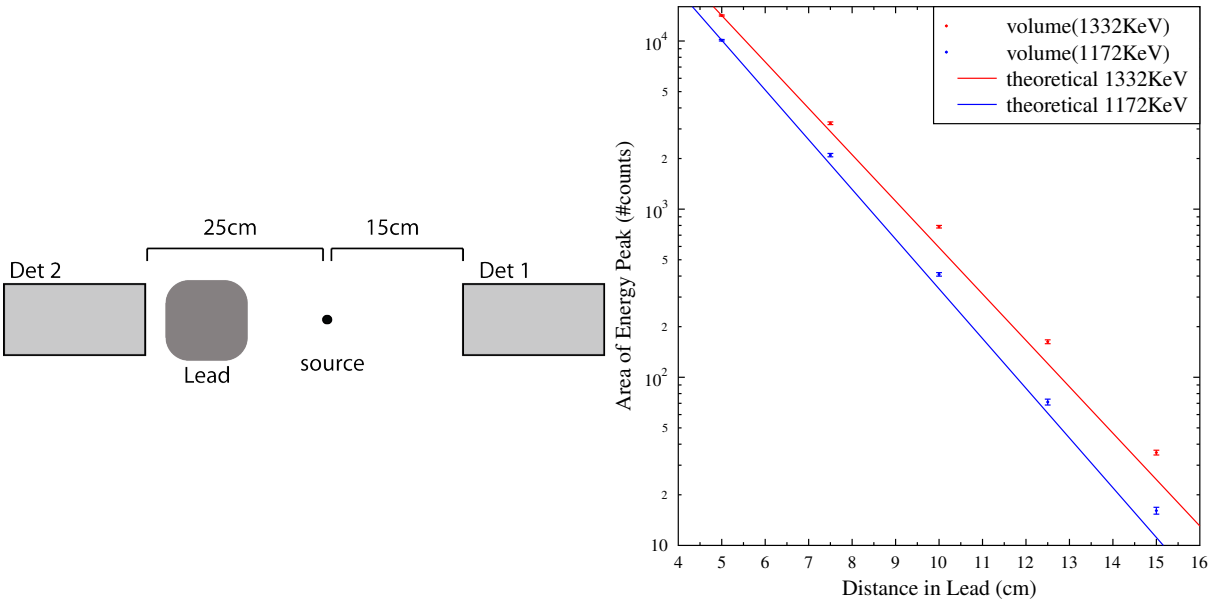

Figure 3.7: Left: Diagram for the two scintillation detector setup. Right: Attenuation of 1332.5 keV and 1173.5 keV photons through lead

through lead could be observed, as opposed to the scattered photons examined previously. It can be observed in Figure 3.7 that the experimentally measured counts in each energy peak follows the same trend as what is expected by theoretical values. These theoretical values were obtained using the NIST absorption coefficients and calculated in the same manner as shown in Equation 3.2.

Although the experimental data follows the trend shown by the theoretical values, there is still a discrepancy between the net values and theory. Such a result indicates at first glance that the absorption rate of photons over lead distance is correct, however the amount of photons absorbed is not correct. This excess of counts in the measured energy peaks is assumed to be caused by unwanted and/or random coincidence events. With additional conditions applied to the energy spectra, it should be possible to omit the unwanted counts and achieve a much closer fit to the theoretical values.

In order to determine an appropriate lead shielding width to suppress the Compton scattering occurring from the 662 keV, a simulation was done with GEANT4 [1]. The simulation was done with two detectors placed at 72° from each other, with a varying lead shield width. From the simulation, it as observed that approximately 10^6 events are absorbed by 20 mm of lead. It was then decided to take a safe approach and choose 7.5

cm of lead to be the minimum width of lead shielding allowed.

3.3 Random Coincidences

In any coincidence experiment it is always important to understand the contribution of random coincidences, or more specifically the random coincidence time rate. A typical timing spectra for the two-photon event would present a peak centered around Δt=0 sitting on a non-zero flat distribution of events. The underlying flat distribution within the time window is due to random time coincidences, while the peak is due to the two-photon event and background events.

In order to correct for this timing background one must set a gate of width τ around the peak, and another two gates of width τ' on the flat background. All events which fall within the τ window are used to create a summed energy spectrum containing both random and true coincidence events. The corresponding energy spectrum from the τ' time gates are scaled with a factor of $\tau/2\tau'$ and then subtracted from the first energy spectrum. The resulting sum energy spectrum, after random coincidence subtraction, is representative of only true coincidence events. The present error due to performing this correction is taken as the ratio of the number of counts in the two-photon coincidence peak and the square root of the number of random coincidences in the time window τ.

The rate of random coincidences within the time gate τ is described by Knoll [23] as

$$\begin{aligned} R_{\text{rand}} &= \tau \cdot R_1 \cdot R_2 \cdot f \\ &= \tau \cdot \epsilon^2_{\text{tot}}(662 \text{ keV}) \cdot R^2_{1\gamma} \cdot f, \end{aligned} \tag{3.3}$$

with R_1 and R_2 representing the singles counting rate of detectors 1 and 2 respectively. For the purpose of this analysis both counting rates are assumed to be the same. ϵ^2_{tot} is the total efficiency of the $LaBr_3$ detector for an incident photon energy of 662 keV, and $R^2_{1\gamma}$ represents the number of 662 keV photons emitted from the source per second. Setting $f = 1$ represents the total random rate, in this experiment however, only the sum energy between 652 and 672 keV is of interest. This energy gate reduces the count rate by a constant factor f determined experimentally to be $f \simeq 13$.

The two-photon rate can be described as

$$R_{2\gamma} = \epsilon_{\text{full}}(E_1) \cdot \epsilon_{\text{full}}(E_2) \cdot R_{1\gamma} \cdot b \tag{3.4}$$

using the full energy efficiencies at energies E_1 and E_2, with the condition $E_1 + E_2 = 662$ keV. The constant 'b' is the branching ratio of the two-photon decay. The error introduced by the subtraction of the random coincidences is given by the ratio

$$\frac{\sqrt{R_{\text{rand}} \cdot t}}{R_{2\gamma} \cdot t} = \frac{\sqrt{\tau} \cdot \epsilon_{\text{tot}}(662\text{keV}) \cdot f}{\epsilon_{\text{full}}(E_1) \cdot \epsilon_{\text{full}}(E_2) \cdot b} \cdot \sqrt{t} \tag{3.5}$$

with t being the experimental measurement time.

It is interesting to note that the source strength factor cancels out in the numerator and denominator. Equation 3.5 also shows that the ratio scales inversely to the square of the distance between the radioactive source and the detector.

3.4 Experimental Advantages of ^{137}Ba

Although there is no very specific reason to favor a ^{137}Cs source, decaying to ^{137}Ba , over any other, there are a few reasons which cause it to be an interesting candidate for the experiment. ^{137}Cs is a radioactive nucleus with a relatively long half-life (∼30 years). As the experiment will spawn over a period of weeks, it is important for the source activity to remain constant, relatively speaking, in order to simplify the analysis. The decay of ^{137}Cs produces only one main γ-ray at an energy of 661.7 keV, which consequently is not in coincidence with any other energy.

The 661.7 keV line is also interesting as it, and it's ∼331 keV two-photon counterpart, is high enough to remain distinctly outside of low energy experimental background. This makes it possible to ignore the low energy signals which arise from background. In addition, a Compton scattered 661.7 keV photon is of low enough energy to be stopped by a fairly small lead shield; thus allowing for a more confined experimental setup.

Additionally it was mentioned earlier that the excited state of ^{137}Ba is a nuclear isomer, that is, has a relatively long lifetime of ∼2.5 minutes. As the one photon transition is

slightly suppressed due to the required high spin change, it can be argued that this provides a more favorable setting for the two-photon process. This argument however would need the backing of a rigorous theoretical calculation on the subject.

3.5 Experimental configuration

As the two-photon branching ratio for the $1h_{11/2}{}^{-} \rightarrow 2d_{3/2}{}^{-}$ transition in ^{137}Ba is predicted to be $2.06 \cdot 10^{-6}$, that is about six orders of magnitude less likely than the single photon decay; it is important to suppress the contributions of the single photon decay. Both types of Compton scattering events were discussed in section 3.1, direct Compton scattering can be suppressed by proper and careful placement of lead shielding. Lead was chosen as a shield for Compton scattering due to its characteristics as an excellent photon absorber, caused by its high density and Z value. The lead thickness between each detector for the first experiment was set to be 12.5 cm. For the second experiment, a lead shield width of 7.5 cm was used.

In the case of the first two-photon experiment, 5 $LaBr_3$ detectors were setup in a steel support frame. Each detector was placed at an angle of 72° from each other, and at a distance of 22 cm from the radioactive source. The solid angle of each detector was mapped out within the detector apparatus, afterwards lead was placed between each detectors. Care was taken to avoid having lead placed within any of the detector solid angles. In order to have the maximum amount of lead between each detectors, lead bricks were shaped to fit ideally the experimental setup.

To perform this experiment, the detectors were grouped up in pairs of 72° and 144° . Any other pairs would not have enough lead between them to stop Compton scattering. The use of multiple similar pairs creates the option to acquire more data in a situation where very few events would be recorded. Through experimental geometry, 5 pairs of 72° and 5 pairs of 144° were formed.

A secondary experiment had two pairs at 96° and one pair at 120°, with all detectors placed at 15.5 cm from the source. The second stage of this setup consisted of three detectors, each placed at 120° from each other.

Each detector was fed by one of three N1470 high-voltage power supply modules.

These modules were used to power both the $LaBr_3$ detectors and the plastic scintillators. The ten detector signals were amplified through an in-house time-filter amplifier (TFA) at Technische Universität Darmstadt. The amplified signals were then fed into the Struck SIS3316 digitizer module. This particular digitizer has a sampling rate of 250 MHz and a resolution of 14 bits. The incoming signals are processed online by one of the digitizer's on board FPGA. With these the energy and time information are extracted from the signals.

Each time the digitizer records an incident event, a trigger signal is sent to the RIO4 module which begins reading out the signal data through the VME backplane. The data is sent through an Ethernet connection and saved on a hard disk. The dead time of the data acquisition system was determined to be less than one percent of the total rate ($\sim$23 kHz). The digitizer utilizes two memory buffers, allowing for overall simultaneous readout and writing of data.

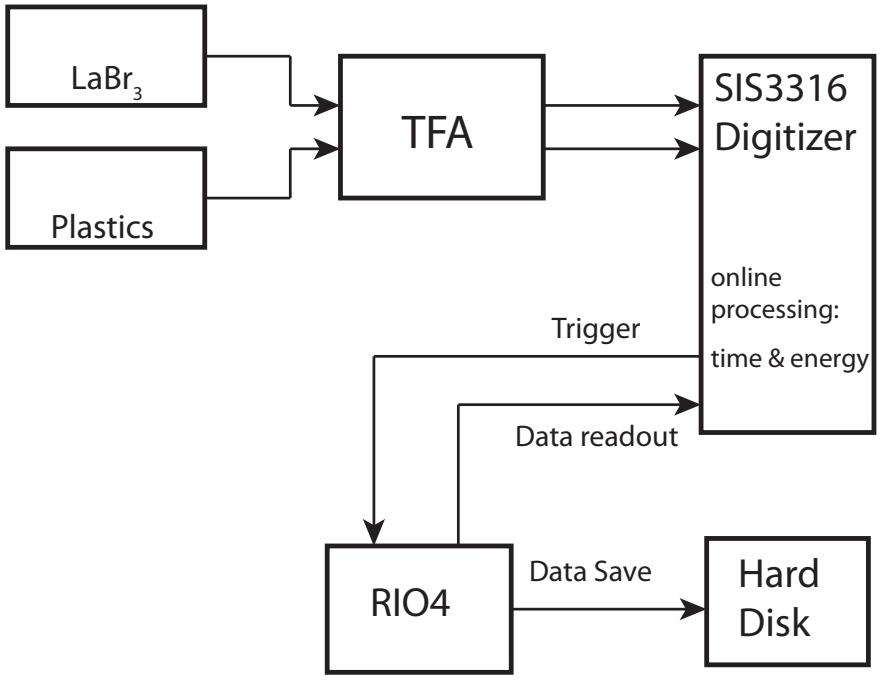

Figure 3.8: Electronic setup for the two-photon experiment.

Digitizer Processing

An incoming signal to the digitizer will have a pulse length of approximately 200 ns and will have a height on the order of millivolts. From this signal, both the energy and timing information must be extracted by the digitizer. In order to extract the timing information from the spectra a CFD algorithm is applied to the signal. From this processed signal a value for the signal time is recorded and stored in a timing array (often represented in this experiment by t[#]). The timing value assigned to the pulse is taken from the digitizer's internal clock. The clock is automatically started when the ADC is turned on and is stopped when it is powered down. The last few bits of the digital clock are stored in a timing variable, which is then used as the absolute timing value. It is important to note that during the experiment only the time difference between two detectors is ever used, therefore this 'inexact' absolute timing values is excusable as only relative timing is important.

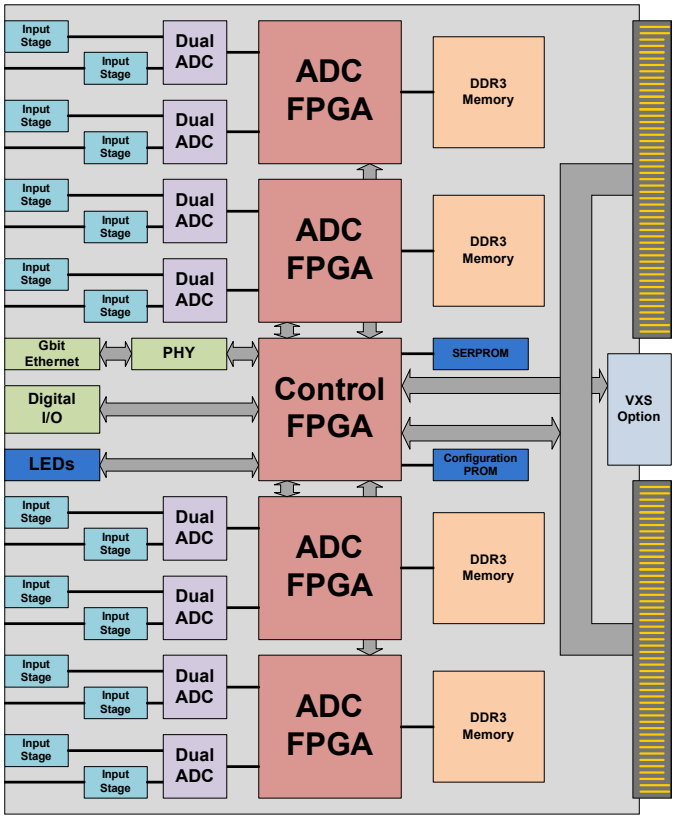

Figure 3.9: Block diagram for the struck SIS3316 digitizer. Image taken from the digitizer user manual [5].

In order to obtain the energy information from the signal, the pulse must be integrated over it's full range. Since this process is being applied in a digital framework, and not analog, a continuous integration over the signal is not possible. The alternative is to create a sum over each sampled point on the peak. With a digitizer sampling at a rate much faster than the signal length, it is possible to assume the sum over all points approaches the expected value from a full signal integration. The obtained energy values are then places in a histogram under the label of 'channels', which must later be calibrated in terms of energy.

In order to obtain a a highly precise timing resolution, the signal is process via an on board digital CFD algorithm. It is the utilization of this 'time filter' on the signal's timing information which permits the measurement of the signal's position to a high, and repeated, precision. Using such a method, STRUCK reports being able to obtain a sub 70 ps timing resolution [5].

In the case of the SIS3316 digitizer, there are eight dual ADC, each treating the signals arriving from two channels. Four ADC FPGAs are connected to two ADCs each, and a DDR3 memory chip for temporary information storage. Using the VME back panel, the Control FPGA communicates with the RIO4 system, which is programmed to interface with the Control FPGA output. In turn, the Control FPGA talks to the other four ADC FPGA, which feed the information previously stored in the DDR3 memory back to the Control FPGA, and ultimately to the RIO4 device.

Chapter 4

Data Analysis and Results

In order to analyze the saved data from the digitizer, the data is first 'unpacked' with ucesb [25] from lmd file formats into root file format [26]. Each lmd file consequently creates a ROOT tree with the timing and energy information for each event observed by every detector in the experimental setup. Through further analysis, these ROOT trees may be combined and analyzed in order to extract the overall run information.

4.1 Energy Calibration & Efficiency Stability

As the two-photon experiment requires many days of consecutive measurements, it is important to consider environmental variations within the lab which would impact the measurements. The greatest effects to consider are the temperature, and potential electric load variation throughout the measurement period. The gain of each detector signal depends on the ambient temperature, in this case the room temperature. It also easy to imagine that the room temperature will not stay perfectly constant throughout a measurement time of multiple days. As such, in order to obtain an optimal energy resolution, it is necessary to calibrate the detectors multiple times a day.

The In Situ calibration was performed using a two-point calibration using the 662 keV transition and an X-ray with an energy of 73 keV. Given the low energy range examined in this experiment, the dependence of the integral of the detector signal on the gamma-ray energy is assumed to be linear. Using this In Situ calibration allows the use of the experimental data for energy calibration, avoiding the need to constantly halt measurements to perform energy calibration. The calibration and efficiency determination is determined at the end of each lmd file, resulting in a calibration and efficiency determination every $\sim$40

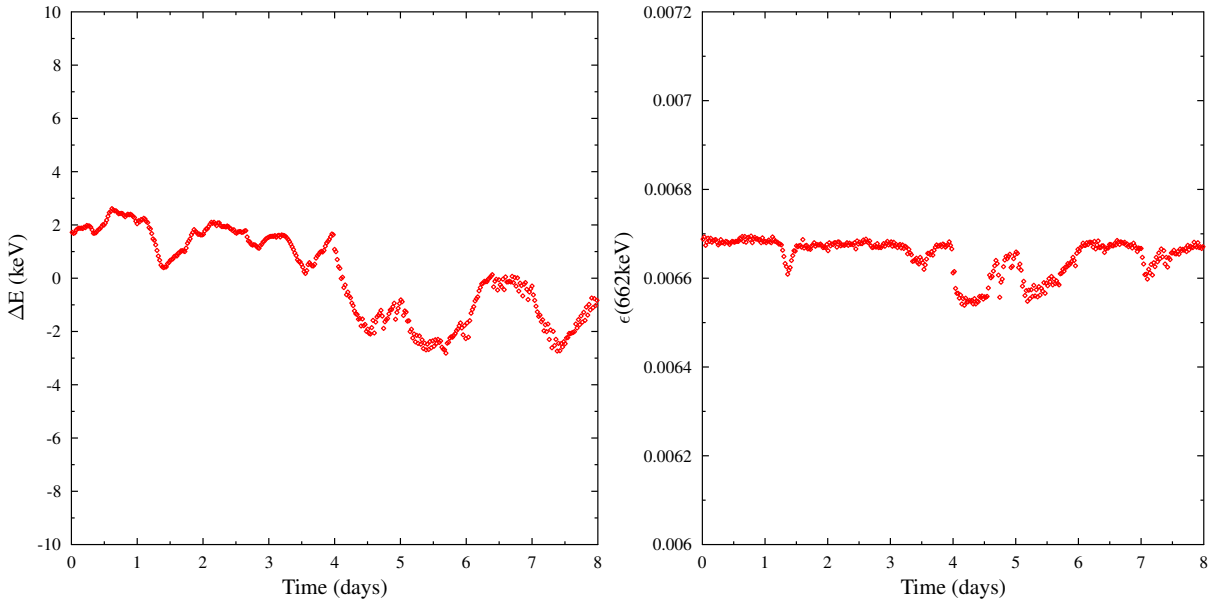

Figure 4.1: Long term variation of the calibration and efficiency values throughout an experimental run. On the left side the uncorrected energy shift for the 662 keV peak is shown. The right hand figure shows the variation of the absolute efficiency throughout an experimental run.

minutes, using the singles spectra of each detector. After application of this calibration, the energy resolution is found to be 2.9-3.1% (FWHM) at the 661.7keV peak.

Observing the two displayed variations in Figure 4.1, it is clear that a fluctuation does occur over time, this fluctuation is however minimal. In the case of the energy variation, a shift of a few keV is observed, however the resolution was earlier stated to be ~ 20 keV. Similarly, the shift in detector efficiency is observed to change only by $\sim 2\%$. Overall, the experimental setup is thus considered stable in terms of energy calibration and efficiency.

In order to obtain an accurate value for the two-photon decay branching ratio, it is necessary to know the absolute efficiencies of each utilized detectors. The determination of detector efficiency is performed automatically with each processed lmd file. The source strength is assumed to stay constant for the duration of the measurement. As the source of use was a 487.9 kBq ^{137}Cs source, with a half life of ~ 30 years, this assumption should be valid for a one to two month long series of measurements.

From the determined efficiencies, it is possible to determine the coincidence efficiency. This coincidence efficiency represents the efficiency that both photons resulting from the two-photon decay are detected by the experimental setup. The coincidence efficiency may

be derived from the single efficiencies given by

$$\begin{aligned} \epsilon(E_1) &= \epsilon_A(E_1) + \epsilon_B(E_1) \\ \epsilon(662\text{ keV} - E_1) &= \epsilon_A(662\text{ keV} - E_1) + \epsilon_B(662 - E_1), \end{aligned} \tag{4.1}$$

where ϵ_A and ϵ_B represent the efficiencies of detectors A and B. From these the product can be determined to be

$$\begin{aligned} \epsilon_{\text{coincidence}}(E_1) &= \epsilon_A(E_1) \cdot \epsilon_A(662 - E_1) + \epsilon_B(E_1) \cdot \epsilon_B(662 - E_1) + \\ &\quad \epsilon_A(E_1) \cdot \epsilon_B(662 - E_1) + \epsilon_B(E_1) \cdot \epsilon_A(662 - E_1) \\ &= \epsilon_A(E_1) \cdot \epsilon_B(662 - E_1) + \epsilon_B(E_1) \cdot \epsilon_A(662 - E_1). \end{aligned} \tag{4.2}$$

The first and second term in Equation 4.2 do not contribute in this experiment as they represent occasions where both photons would be captured by the same detector. Thus $\epsilon_{\text{coincidence}}(E_1)$ is shown to depend on the energy sharing of both emitted photons.

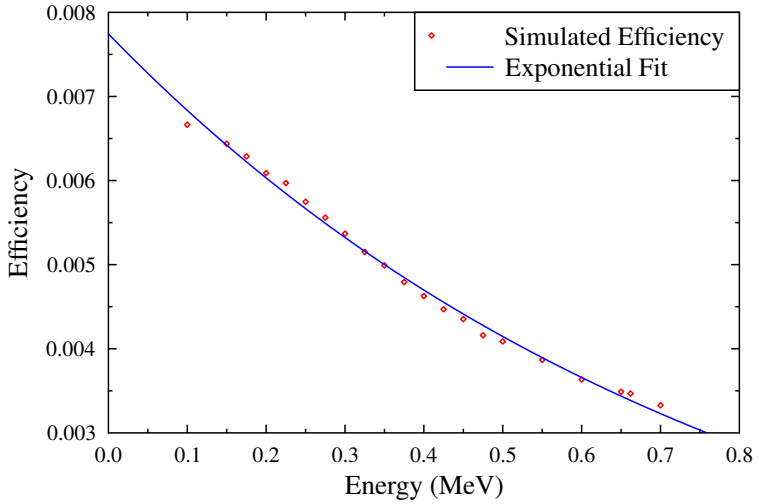

Figure 4.2: Fit line applied to the simulated efficiency values (from GEANT4), as well as the measured efficiency. The adjusted fit line is not shown for the sake of cleanliness. The variation in efficiency values is due mainly to the simulated detector distance being different than that used for the experimental value.

Within these experiments, the widest energy range considered is $|E_1 - E_2|$ <200 keV

(described in section 4.5). Due to this limited region of interest, it is possible to use a fit equation for the simulated efficiencies of the form $\epsilon(E) = a \cdot \exp(-b \cdot E)$, shown in Figure 4.2. The benefit of using such an equation to fit the efficiencies, as opposed to the typical $\epsilon(E) = a + b\log[E] + c\log^2[E] + ...$, arises from the product of two efficiencies (or the coincidence efficiency). For the operation

$$\epsilon^i_{\text{coinc}} = 2 \cdot \epsilon_A \cdot \epsilon_B$$

using the exponential fit, the end result is independent of E_1. In order to obtain the energy independent result, it is important that the energy in detector A and B are not independent of each other, in fact if $E_A = E_1$, then $E_B = 661.7$ keV $- E_1$ for the case of the 662 keV decay from ^{137}Ba . As such we obtain

$$\begin{aligned}
\epsilon_A \cdot \epsilon_B =& (a_A \exp(-b_1))(a_B \exp(-b_2)) \\
=& a_A a_B \exp(-b(E_1 + E_2)) \\
=& a_A a_B \exp(-b(E_1 + (0.662 \text{ keV} - E_1))) \\
=& a_A a_B \exp(-b \cdot 0.662 \text{ keV})
\end{aligned}$$

Both coefficients a and b where determined via a least squares fit on the simulated efficiencies by GEANT4 shown in Figure 4.2, and evaluated to be $a = 0.0077$ and $b = 1.25$. These simulated efficiencies where determined for detectors 22 cm away from a ^{137}Cs source, it is therefore important to scale the fit equation in order to have it represent the experimental detector distance. This scaling was done by adjusting the simulated 662 keV point to an experimentally measured value at 662 keV for each detector. The scaling will present no change to the factor b, the factor a is however now unique to each detector, resulting in a final coincidence efficiency equation defined as

$$\epsilon^i_{\text{coinc}} = 2a_A a_B \exp(-1.25 * 0.662) \tag{4.3}$$

4.2 Correction for the Time Random Coincidences

It was explained in section 3.3 that the time random coincidences need to be subtracted from the measured spectra. The $LaBr_3$ detector pairs were time-aligned using information gathered by performing a measurement with a ^{60}Co source. The use of a ^{60}Co source is ideal for time alignment due to its simultaneous emission of a 1332 keV and 1173 keV gamma rays. As both of these gamma rays are emitted simultaneously they should arrive in their respective detectors at the same moment. Analyzing the event files however often shows a time offset between the times of arrival. These time offsets can be caused by numerous factors such as cable length, photomultiplier setup, slight differences in amplifier setup, etc... Using these offsets, the detector pairs are 'time-aligned' to represent the simultaneous arrival of both ^{60}Co gamma rays. This time-alignment factor is then kept for the analysis of the two-photon decay.

In order to subtract the random counts from the true coincidence spectra, a time gate (τ) of 2.4 ns was applied around the coincidence peak. The small width of the gate was chosen in order to avoid selecting any potential sequential Compton scattering as well as to minimize the error in the random subtraction process. Two additional gates (τ') of 56 ns were applied on the flat random distribution on the left and right side of the coincidence peak.

An energy spectra is obtained for both of these time gates, the τ spectra shaped by the true coincidence events along with the random event, while the second spectra (τ') is shaped only by random coincidences. The sum energy spectra of the random coincidences is then scaled by a factor of $\tau/(2\tau')$ in order to correct for the different time gate lengths. The final sum energy spectra can then be obtained by subtracting the first curve by the second one.

A direct consequence of selecting a 2.4 ns time gate around the peak is the partial rejection of real two-photon events. In order to correct for these missing events, a measurement of a ^{60}Co source is done with the same experimental setup and similar analysis conditions. The reasoning for choosing a similar time gate is to remove any potential error from energy resolution variation. Using the first 5 $LaBr_3$ detector setup, it was measured

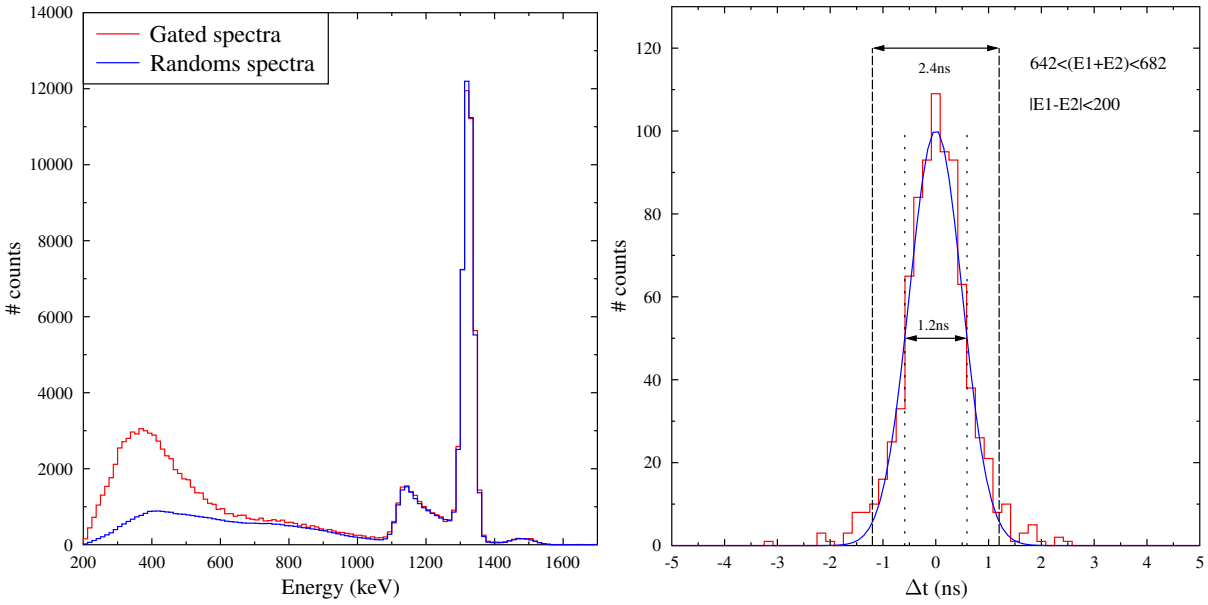

Figure 4.3: Left: Sum energy spectra of the events satisfying the random (blue) and true (red) coincidence time conditions. The random spectra is corrected to account for the wider time gate. Right: ^{60}Co timing spectrum determined with similar conditions than those applied to the 662 keV timing peak. Additional value of FWHM and 2.4 ns time gate are represented.

that the number of omitted events by this time gate was approximately ∼10%.

4.3 Background Correction

The issue of background radiation was presented in chapter 3. It is important to keep track of the measured background levels per angle pairs as the measured levels does not remain constant for each angle. In the experiment of Ref.[1], it was observed that the background radiation in the 144° pairs was a factor of ∼6 less than in the 74° pairs. In the second experiment, the 120° pair had a factor of ∼ 3 smaller than the 96° detectors. This variation in background is due to the larger distance between detectors of greater angles. Another setup was attempted at ∼40°, however the background rate was once again too high, most likely due to the close positioning of each detector pair.

In order to limit the background radiation, lead shielding was placed around the setup as well as above the detectors. In addition to the passive lead shielding, plastic scintillators were added above the $LaBr_3$ detectors. The use of the plastic scintillators as vetos,

successfully reduced the amount of background events by a factor of ∼2.

In order to better reduce the background levels, a more in depth understanding of origin for the entire background events would be required. At the moment of this experiment however, it is possible to construct experimental setups with sufficiently few background events.

4.4 Timing Analysis

It is clear that there is a peak found at 662 keV (see Figure 4.7), which seems to satisfy the conditions which have been applied to the experiment. It has so far been assumed that these values for the angular distribution are due to the two-photon decay, however an experimental demonstration that the measured value is not due to Compton scattering is still needed.

A previous statement was made arguing that the lead shielding of 7.5 cm between each detector pair is sufficient to block direct Compton scattering. This was supported by calculations demonstrated earlier as well as a GEANT4 simulation. These arguments by themselves are strong, but a more direct demonstration is desirable.

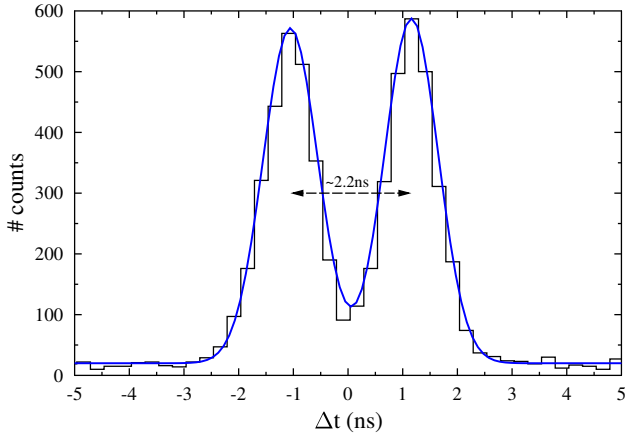

Figure 4.4: Timing difference plot for Compton scattering observed between two detectors with no lead shielding. The distance between both detectors are ∼33 cm.

Although the $LaBr_3$ detectors have an excellent timing of ∼1.2 ns around the 662 keV

region, this is not precise enough to offer a very clear distinction between the direct Compton scattered events and the two-photon events. That being said, this timing resolution does permit to gather information on the timing spectrum shape and thus determine if the peak seen at 662 keV is due to Compton scattering or due to the two-photon decay.

The timing plot shown in Figure 4.4, and as well in the subsequent plots, represents the timing difference between two detectors. In Figure 4.4, the timing of detector 0 is subtracted from that of detector 1 (t[0]-t[1]). The visible double peak structure comes from the two Compton scattering timing possibilities. The peak centered around 1.1 ns occurs when a gamma-ray scatters from detector 1 into detector 0. Consequently the peak centered around -1.1 ns represents events where a gamma-ray scatters from detector 0 into detector 1.

Thus the peak separation of $\sim$2 ns is representative of light traveling a distance of $\sim$33 cm. One would expect that light, in a normal setting, would take approximately 1ns to travel 30 cm. This timing corresponds roughly with what is observed in Figure 4.4.

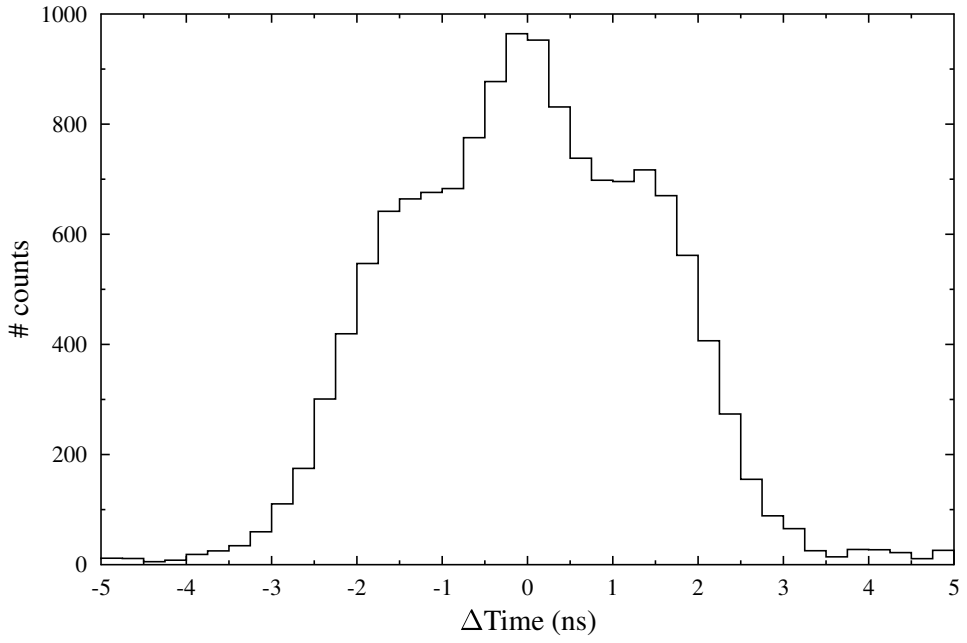

Figure 4.5: Timing difference spectrum representing random coincidences and true two-photon coincidences. The peak subtraction is done solely via subtracting the shown spectra by a purely random spectra.

In order to observe the timing spectra corresponding to the 662 keV energy peak, the

energy condition of 649 keV <(E1+E2)< 675 keV is applied on the sum energy spectra. The time difference for any coincidence events satisfying this sum energy condition is recorded, and shown in histogram form in Figure 4.5 on the right side. It is important to note that the spectrum shown on the right side of Figure 4.5 is caused both by two-photon events and random events. It is thus necessary to subtract out these random events, shown on the left side of Figure 4.5, in order to obtain a timing spectrum representative of only the two-photon events. This subtracted timing spectrum is shown in Figure 4.6.

For the case of 120° analyzed here, the average distance which a Compton scattered photon would have to travel would be ∼33 cm. As such one would expect, if Compton scattering events are present, to have two peaks present at ∼ ±1.1 ns in the timing spectra. These two potential peak positions are represented by the two vertical doted lines in the figure. It is clear from Figure 4.6 that there is no peak present at either positions. Within the figure a timing peak around Δt=0. Although this does not rule out Compton scattering entirely, it does rule it out as a main contributor to the sum energy peak observed at 662 keV.

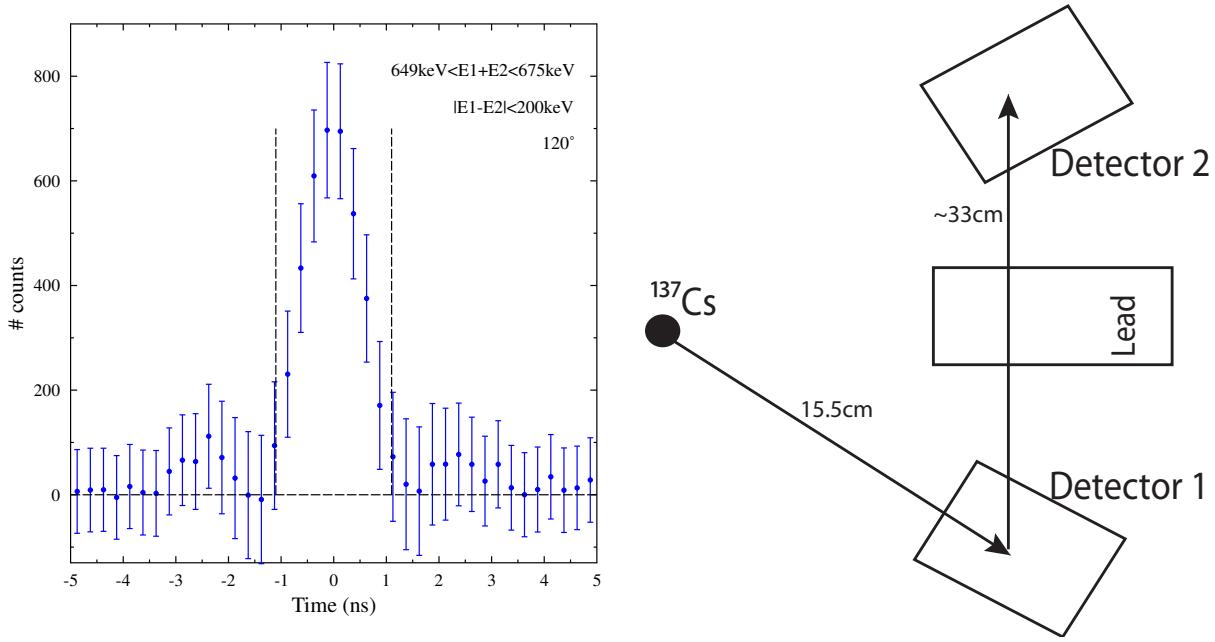

Figure 4.6: Left: Subtracted timing spectrum with randoms subtracted from the full timing spectra. The timing spectra clearly shows a single peak centered around Δt=0, and an absence of peaks close to the doted lines which would represent Compton scattering. Right: Rough diagram of a 120° detector pair with utilized distances, representing the path a direct Compton scattered ray would take.

4.5 Determining the Branching Ratio

If we 'zoom-in' into the region of interest (close to 662 keV) in Figure 4.3, it is already evident that there is a peak present. It is however still necessary to subtract out the random coincidences and provide a valid fit which accurately represents the background and the peak. The error bars for the random coincidence sum energy spectra are considered negligible due to the very large time gate of 112 ns, compared to the small gate of 2.4 ns used on the coincidence peak.

In order to fit the background of the subtracted spectra (see Figure 4.7), the background function was defined as $Bckg(x) = \exp(a + b(x-c) + d(x-c)^2)$ with x being the energy of the subtracted spectra in keV. The complete fit function used to define the area shown in Figure 4.7 was the sum between the background and a typical Gaussian function. The width of the Gaussian was kept constant at 20.2 keV, which is the determined average energy resolution of the $LaBr_3$ detectors at 662 keV (from the single emission spectra).

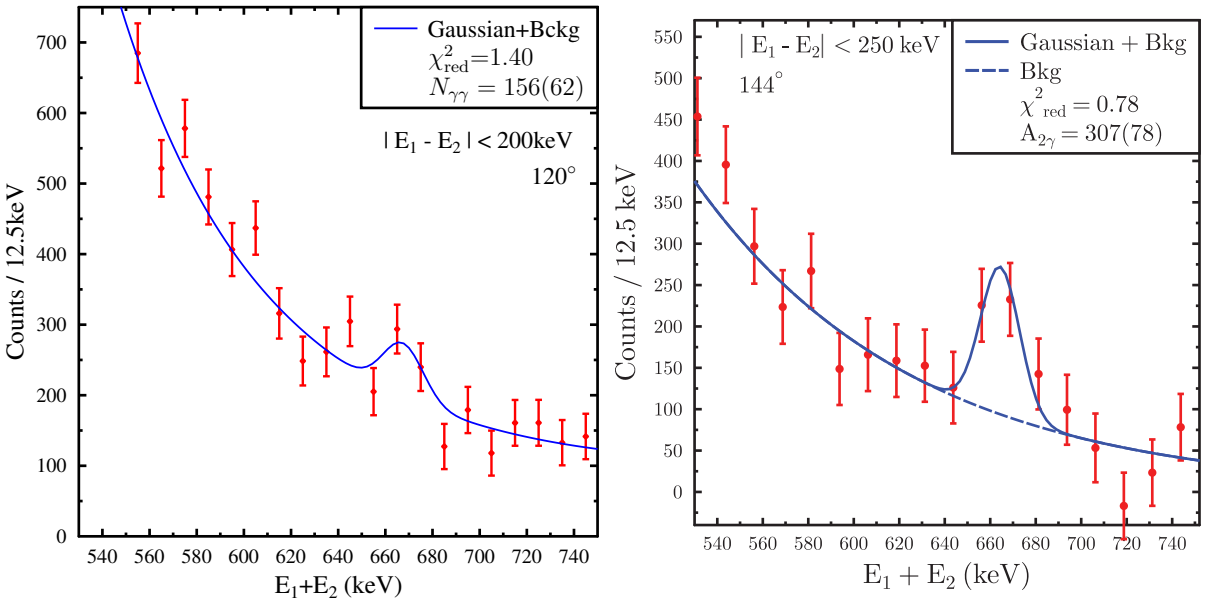

Figure 4.7: Left: Final subtracted spectra for the angle of 120° with an energy gate of $|E_1 - E_2| < 200$ keV in order to suppress a portion of the sequential Compton scattering. Right: Final subtracted spectra for 144° with the energy gate $|E_1 - E_2| < 250$ keV. Right image taken from Ref.[1]

To reduce the effect of the broad peak present in front of the desired two-photon peak,

whose origin is not yet known, the energy gate $|E_1 - E_2|$ <200 keV was applied to the energy spectra. For the case of the 72° and 144° experiment, the energy gate was set as $|E_1 - E_2|$ <250 keV due to a lower effect from the preceding curve. The energy gate of 200 keV (250 keV) rejects the energies below ∼231 keV (∼206 keV), and above ∼431 keV (∼456 keV).

Although the results for the 72° (and 144°) proved very nice with a $\chi^2_{\text{red}} = 0.76$ [1], the 120° measurement proved less ideal with $\chi^2_{\text{red}} = 1.40$ and $N_{\gamma\gamma} = 156(62)$ for a measurement time of 35 days. The cause for the poor fit at 120° is due to the the much higher sequential Compton scattering background than that observed at 144° .

It is clear that the subtracted peak shown for the 120° subtracted spectra is far from ideal. The current curve fitting show in the left plot of Figure 4.7 is taken to be acceptable due to the previous fitting of the 72° and 144° data sets. The 144° subtracted spectra is shown on the right side of Figure 4.7, where a much clearer peak is visible. The same peak characteristics which are clearly visible for the 144° peak, are then possible to observe in the 120° peak.

The subtracted energy spectra shown in Figure 4.7 and Figure 4.3 for 120° show a much greater influence of the lower energy sequential energy distribution than was observed at 72° and 144° . This is believed to be in part due to having the detectors placed closer to the source for the 120° than they had been for the 72° and 144° run, as well as a lack of customized lead bricks. By comparing the left and right plots of Figure 4.7, it is clear that a reduced background would have allowed for a similar fit than that obtained for 140° .

During the experimental process of determining 120° , an attempt was made to measure the branching ratio for an angle of 96° . During the course of the experiment however a flaw in the lead shielding and detector configuration was found. Due to this issue, the information obtained for these angle pairs was not acceptable for analysis, therefore no analysis of the 96° branching ratio was performed.

We begin the derivation for the 2γ branching ratio with the emission of a single photon for a given radioactive source.

$$N_\gamma = \epsilon(662 \text{ keV}) R_s t \tag{4.4}$$

Where R_s is the radioactive source strength, t is the measurement time, and $\epsilon(662\text{ keV})$ represents the full energy efficiency at 662 keV for any detector. It is possible to the adapt this equation to the two-photon emission as.

$$N_{\gamma\gamma} = \epsilon_{\text{coinc}} R_s t \frac{\Gamma_{\gamma\gamma}}{\Gamma_\gamma}$$

Where $\epsilon^i_{\text{coinc}}$ represents the coincidence efficiency for each detector pair, and was defined in Equation 4.3. It is then possible to re-arrange the equation in order to solve for the branching ratio.

$$\frac{\Gamma_{\gamma\gamma}}{\Gamma_\gamma} = \frac{N_{\gamma\gamma}}{\epsilon_{\text{coinc}} R_s t}$$

Substituting Equation 4.4 into the previous equation one obtains a value for the branching ratio independent of time and source strength.

$$\frac{\Gamma_{\gamma\gamma}}{\Gamma_\gamma} = \frac{N_{\gamma\gamma} \cdot \epsilon(662\text{ keV})}{\epsilon_{\text{coinc}} \cdot N_\gamma} \tag{4.5}$$

Equation 4.5 represents the branching ratio as one would calculate from one pair of two detectors. In an experiment consisting of multiple pair, one must sum over each detector pairs resulting in the equation

$$\frac{\Gamma_{\gamma\gamma}}{\Gamma_\gamma} = W(\theta) \frac{N_{\gamma\gamma} \cdot f \cdot \sum_{i=1}^{n} \epsilon_i(662\text{ keV})}{\left(\sum_{i=1}^{n} N^i_\gamma\right) \cdot \left(\sum_{i=1}^{m} \epsilon^i_{\text{coinc}}\right)}, \tag{4.6}$$

where $W(\theta)$ represents the angular correlation function, describing the variation of branching ratio value with respect to the two-photon angle separation.

Throughout the full experimental run, it was required on multiple occasions to remove the ^{137}Cs source. As it is not possible to replace the source to the identical initial position, the efficiencies must be adapted accordingly. In order to do this, an average efficiency was determined for each run, after which an overall efficiency average was performed by performing a time weighted average of each run's average efficiency.

The factor f is defined as the sum of two other factors, f_t and f_e. The f_t factor corrects the $N_{\gamma\gamma}$ term for the events left outside of the 2.4 ns time gate on the two-photon

peak. Using the method described in section 4.2, the timing factor is determined to be $f_t = 1.065$.

The applied energy gates of 200 keV (and 300 keV) rejects certain photon energies from the peak area $N_{\gamma\gamma}$. In order to correct for these terms, the integral of the full angular function is divided by the energy limited integral of the same angular function. For the energy gate of 200 keV (300 keV), the quadrupole-quadrupole factor is determined to be $f_e = 1.42$ ($f_e = 1.12$) and for the dipole-octupole $f_e = 2.40$ ($f_e = 1.54$).

Due to the small uncertainty in each distance between the source and detectors, as well as the small uncertainty in the source strength, the detector efficiency uncertainty is assumed to be around 2%. The uncertainty in the total amount of counts in the 662 keV counts is negligeable as well with a total counts on the order of 10^4. The dominant uncertainty of the $N_{\gamma\gamma}$ value is taken from the fit results which takes into account errors with the background function.

It is now possible to determine the values for Equation 4.6 where the raw experimental branching ratio $((\Gamma_{\gamma\gamma}/\Gamma_\gamma)\cdot W(\theta))$ for 120° is determined to be $0.55(22)\cdot 10^{-6}$. It is also possible to determine the values for each value of f_e, that is assuming a pure dipole-octupole (do) or quadrupole-quadrupole (qq) transition. The results for the 120° measurements, as well as those previously determined for the 72° and 144° are shown in Table 4.1.

Branching Ratio	120°	72°	144°
Experimental	$0.55(22)\cdot 10^{-6}$	$1.56(23)\cdot 10^{-6}$	$0.70(18)\cdot 10^{-6}$
quad.-quad.	$0.79(31)\cdot 10^{-6}$	$1.75(27)\cdot 10^{-6}$	$0.85(22)\cdot 10^{-6}$
dip.-oct.	$1.33(53)\cdot 10^{-6}$	$2.40(36)\cdot 10^{-6}$	$1.33(35)\cdot 10^{-6}$

Table 4.1: Summary of the branching ratio $(\Gamma_{\gamma\gamma}/\Gamma_\gamma \cdot W(\theta))$ values for the two-photon decay experiment. The results for the various angles are obtained with |E1-E2| <X. In order to determine the values for the angles 72°, 120°, and 144°, the utilized values of X are 300 keV, 200 keV, and 250 keV respectively. The values for 72° and 144° are taken from Ref.[1]

Figure 4.8 clearly demonstrates a clear discrepancy between the measured values of the two-photon branching ratio and the theoretical models which assumer pure quadrupole-quadrupole or dipole-octupole transitions. The most likely cause for this variation is due to the assumption that the two-photon decay occurs purely through one of the two

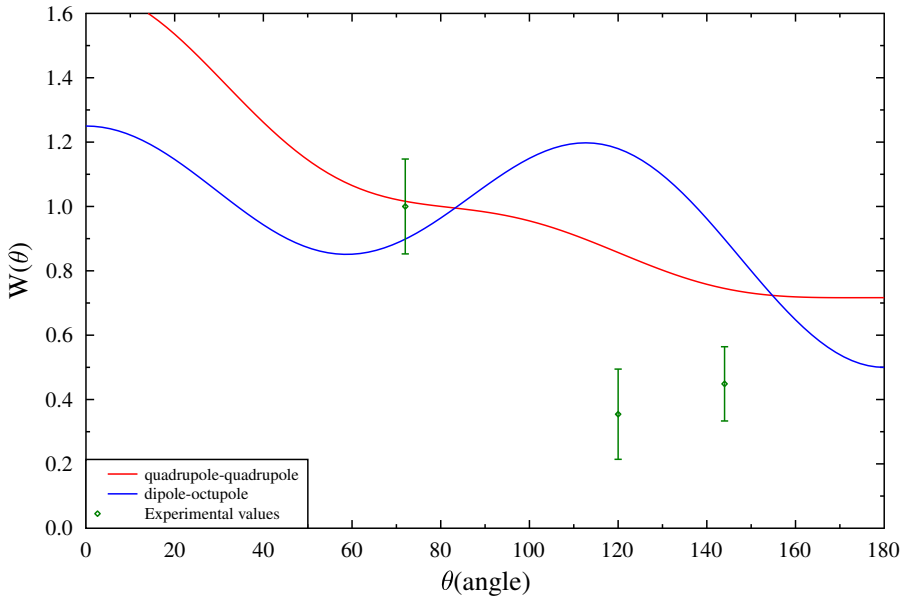

Figure 4.8: Demonstration of the angular distribution $W(\theta)$ measurements and theoretical models. Both theoretical lines and the data points are normalized to the 72° data point.

transitions, whereas it is possible that the decay proceeds via a mixing of states. Such an effect caused by the mixing of states was observed for the $0^+ \rightarrow 0^+$ transition in ^{90}Zr [6]. At the moment, a more accurate theoretical model is needed to represent the angular distribution of the two-photon decay for the ^{137}Ba transition, this is currently being developed by D.J. Millener.

Chapter 5

Summary & Outlook

In this thesis, the feasibility of performing a two-photon analysis on the ^{137}Ba isotope was first analyzed. Making use of the $LaBr_3$ detectors available at the Institut für Kernphysik (IKP) at the Technische Universität Darmstadt, the timing and energy resolution for the setup were determined to be, for the region around 662 keV, to be $\sim$ 20 keV and $\sim$1.2 ns respectively.

The absorption of direct, and Compton scattered ^{60}Co gamma-rays (1173 keV and 1332 keV) in Lead was first examined in order to determined the minimum required width of lead shielding for the experiment. The experimental results were compared to a GEANT4 simulation in order to obtain a parallel between simulated and experimental values. Noting a slight overestimation of absorption from the lead in the GEANT4 simulation, a value of 7.5 cm was chosen as a minimum lead shield width for the experiment. Given that the simulation returned a value of $\sim$3 cm as sufficient to prevent Compton scattering from the 662 keV photon, the increased width of 7.5 cm was deemed thick enough to prevent all direct Compton scattering between any detector pair.

This experiment presented a few significant difficulties, of which notably was Compton scattering and background/random coincidences. With the aid of sufficiently wide lead shielding, direct Compton scattering was suppressed. Appropriate time and energy gates were determined to properly separate out 'sequential' Compton scattering. Although the origin of the entire background radiation was never fully understood, the use of plastic scintillators and appropriate $LaBr_3$ detector placement proved sufficient to allow for a proper measurement. Random coincidences though still proved to be the main factor for the final determined experimental uncertainty.

Using the $LaBr_3$ setup, clear evidence for the two-photon decay from the $\frac{11}{2}^-$ isomeric

state to ground state in ^{137}Ba was observed. The differential branching ratios at angles 72°, 144°, both tken from Ref.[1], and 120° were measured to be $1.56(23)\cdot10^{-6}$, $0.55(22)\cdot10^{-6}$, and $0.70(18)\cdot10^{-6}$ respectively. The energy conditions used were of $|E_1 - E_2| < 250$ keV for 72° and 144° , and $|E_1 - E_2| < 200$ keV for 120°. The results obtained for the three angles do vary from the current theoretical models, which assume an either pure dipole-octupole or quadrupole-quadrupole transition.

A significant increase in background counts was observed for the measurement of 120° as opposed to the 72° and 144° measurements. The increase in background is assumed to be caused by the shorter distance between the detectors and the radioactive source, and consequently a shorter distance between each detectors. With such a shorter path, it is a possibility that more sequential Compton scattered photons triggered both detectors.

The successful measurement of the two-photon branching ratio creates a new means to investigate atomic nuclei. As the decay depends on the sum over all states, it provides a very interesting observable in the world of atomic nuclei. This quantity may thus be equivalent to other important observables such as the diagonal electric dipole polarizability and the diagonal magnetic dipole susceptibility. As such the precise determination of this branching ratio might contribute to solve current fundamental open problems such as restricting the parameters of the equation of state, or accurately determining neutron skin thickness.

The results obtained throughout this experiment are in no way a final step on the subject of the two-photon decay. Following these first, non-restricted, two-photon decay measurements, many more steps may be taken to pursue the subject much more in depth.

- The current experiment stands with three various angles for the branching ration, a continuing step would be to obtain a more rigorous trend in the angular dependence of the branching ratio.

- The measurement of the two-photon decay need not be limited to a ^{137}Cs source. A further measurement of the decay in another source such as ^{54}Mn (a $2^+ \rightarrow 0^+$ transition) could prove interesting as it is a non-isomeric decay. As well, it would be possible to perform this experiment on a more exotic/short-lived source created with a particle accelerator and perform the analysis on site or nearby.

- It might also be possible to utilize a particle accelerator to populate a given state. This might allow to investigate the two-photon decay probability along an isotopic or isotonic chain.

References

[1] Christopher Walz. *The two-photon decay of the 11/2- isomer of 137Ba and mixed-symmetry states of 92,94Zr and 94Mo.* PhD thesis, TU Darmstadt, Darmstadt, July 2014.

[2] Rob Pywell. Electromagnetic transitions. University of Saskatchewan Lecture, http://physics.usask.ca/ pywell/p452/, 2014.

[3] Maria Göeppert-Mayer. Über elementarakte mit zwei quantensprüngen. *Annalen der Physik*, 401(3):273–294, 1931.

[4] Particle Data Group. Review of particle physics. http://pdg.lbl.gov/2011/download/rpp-2010-JPhys-G-37-075021.pdf.

[5] struck innovative system. *SIS3316 Familly, 16 Channel VME Digitizer, 16 Channel Desktop Digitizer.* struck.

[6] J. Kramp, D. Habs, R. Kroth, M. Music, J. Schirmer, D. Schwalm, and D. Broude. Nuclear two-photon decay in $0^+ \rightarrow 0^+$ transitions. *Nuclear Physics*, 474(2):412–450, 1987.

[7] Aage Bohr and Ben Mottelson. *Nuclear Structure. Volume I. Single-Particle Motion.* Benjamin, New York, 1969.

[8] P. Van Isacker. Nuclear charge radii and electric monopole transitions in the interacting boson model. *AIP Conf.Proc.*, 1488:45–52, 2012.

[9] S.G. Nilsson. Binding states of individual nucleons in strongly deformed nuclei. *Matematisk-fysiske Meddelesler*, 29(16):1–69, 1955.

[10] N.D. Cook. *Models of the Atomic Nucleus: Unification Through a Lattice of Nucleons.* Springer-Verlag, 2nd edition, 2010.

[11] W. Pfeifer. *An Introduction to the Interacting Boson Model of the Atomic Nucleus.* arχiv, 1st edition, 1998.

[12] Yang Sun. Projected shell model description for nuclear isomers. *arXiv*, 2008.

[13] Monika Patial, AK Jain, P Arumugam, and Balraj Singh. Atlas of nuclear isomers. *Chart*, 100:120, 2010.

[14] Philip M Walker and James J Carroll. Ups and downs of nuclear isomers. *Physics today*, 58(6), 2005.

[15] J.L Friar. Low-energy theorems for nuclear compton and raman scattering and $0+\rightarrow 0+$ two-photon decays in nuclei. *Annals of Physics*, 95(1):170 – 201, 1975.

[16] A. Tamii, Y. Fujita, H. Matsubara, T. Adachi, J. Carter, M. Dozono, H. Fujita, K. Fujita, H. Hashimoto, K. Hatanaka, T. Itahashi, M. Itoh, T. Kawabata, K. Nakanishi, S. Ninomiya, A.B. Perez-Cerdan, L. Popescu, B. Rubio, T. Saito, H. Sakaguchi, Y. Sakemi, Y. Sasamoto, Y. Shimbara, Y. Shimizu, F.D. Smit, Y. Tameshige, M. Yosoi, and J. Zenhiro. Measurement of high energy resolution inelastic proton scattering at and close to zero degrees. *Nuclear Instruments and Methods in Physics Research Section A: Accelerators, Spectrometers, Detectors and Associated Equipment*, 605(3):326 – 338, 2009.

[17] I. Tews, T. Krüger, K. Hebeler, and A. Schwenk. Neutron matter at next-to-next-to-next-to-leading order in chiral effective field theory. *Phys. Rev. Lett.*, 110:032504, Jan 2013.

[18] A. Tamii, I. Poltoratska, P. von Neumann-Cosel, Y. Fujita, T. Adachi, C. A. Bertulani, J. Carter, M. Dozono, H. Fujita, K. Fujita, K. Hatanaka, D. Ishikawa, M. Itoh, T. Kawabata, Y. Kalmykov, A. M. Krumbholz, E. Litvinova, H. Matsubara, K. Nakanishi, R. Neveling, H. Okamura, H. J. Ong, B. Özel-Tashenov, V. Yu. Ponomarev, A. Richter, B. Rubio, H. Sakaguchi, Y. Sakemi, Y. Sasamoto, Y. Shimbara, Y. Shimizu, F. D. Smit, T. Suzuki, Y. Tameshige, J. Wambach, R. Yamada, M. Yosoi, and J. Zenihiro. Complete electric dipole response and the neutron skin in ^{208}Pb. *Phys. Rev. Lett.*, 107:062502, Aug 2011.

[19] Music.M. *Search for the two-photon decay of the 2+ first excited states in 18O and 28Si*. PhD dissertation, University of Heidelberg, 1986.

[20] D. J. Millener, R. J. Sutter, and D. E. Alburger. 2-gamma decay of the 662-keV isomer in ˆ137Ba. In *APS Division of Nuclear Physics Meeting Abstracts*, page C8, October 2011.

[21] D. J. Millener. Theory for the 2-γ transitions: I. unpublished.

[22] D. J. Millener. Private communication.

[23] Knoll and F. Glenn. *Radiation Detection and Measurements*. John Wiley & Sons, 1st edition, 1979.

[24] The National Institute of Standards and Technology (NIST). http://physics.nist.gov/PhysRefData/XrayMassCoef/ElemTab/z82.html.

[25] A.T. Johansson. The ucesb unpacker generator (unpack & check every single bit). http://fy.chalmers.se/∼f96hajo/ucesb/. Accessed: 15/06/2013.

[26] ROOT Team. Root webpage. http://root.cern.ch/drupal/. Accessed: 27/06/2014.

[27] W.R. Leo. *Techniques for Nuclear and Particle Physics Experiments*. Springer-Verlag, 2nd edition, 1994.

[28] B. Margolis. Two-photon decay and the lifetime of giant resonance states. *Nuclear Physics*, 28(3):524–528, 1961.

[29] G.W.F. Drake, G.A. Victor, and A. Dalgarno. Two-photon decay of the singlet and triplet metastable states of helium-like ions. *Nuclear Physics*, 180(1):25–32, 1968.

[30] S. Harb, K.D. Salahel, and A. Abbady. Study of efficiency calibrations of HPGe detectors for radioactivity measurements of environmental samples. In *Proceedings of the 3rd Environmental Physics Conference*, Physics department, Faculty of Science, South Valley University, 83523 Qena, Egypt, February 2008.

[31] J.C. Verplanke. Full-energy peak efficiency calibration of a well-type Ge(Li) gamma-ray detector. *Nuclear Instruments and Methods*, 96(4):557–560, 1971.

[32] G.A. Kumar, I. Mazudar, and D.A. Gothe. Experimental measurements and GEANT4 simulations for a comparative study of efficiencies of $LaBr_3$:Ce, NaI(Tl), and BaF_2. *Nuclear Instrumentation and Methods in Physics Research A*, 610(2), 2009.

[33] O'Halloran. T, Sokolsky. P, and Yoshida. S. The highest-energy cosmic rays. *Physics Today*, 51(1), 1998.

[34] Gordon Gilmore. *Practical Gamma-Ray Spectrometry.* John Willey & sons, 2nd edition, 2008.

[35] D. J. Millener. Theory for the 2-γ transitions: II. unpublished.

[36] D.P. Grechukhin. Two-quantum transitions of atomic nuclei. *Nuclear Physics*, 35(0):98 – 113, 1962.

[37] A Kuhn, S Surti, KS Shah, and JS Karp. Investigation of labr 3 detector timing resolution. In *Nuclear Science Symposium Conference Record, 2005 IEEE*, volume 4, pages 5–pp. IEEE, 2005.

[38] Steven C. Pieper. Quantum monte carlo calculations of light nuclei. *Nuclear Physics A*, 751(0):516 – 532, 2005. Proceedings of the 22nd International Nuclear Physics Conference (Part 1).